Ab Initio Calculations of Amplitude and Phase Functions for Extended X-ray Absorption Fine Structure Spectroscopy

Boon-Keng Teo* and P. A. Lee

Contribution from Bell Laboratories, Murray Hill, New Jersey 07974.
Received October 16, 1978

Abstract: Extended X-ray absorption fine structure (EXAFS) amplitude and phase functions have been calculated from first principle for K and L edges of nearly half of the elements in the periodic table. It is shown that for $L_{II,III}$ edges, the transition from the initial state to the d final state is favored by almost a factor of 50 over the transition to the s final state such that the $L_{II,III}$ EXAFS can be analyzed in the same way as K and L_I edges with the use of the $l = 2$ phase shifts. These theoretical EXAFS functions exhibit significant new structures (as a function of electron wave vector) which are in accord with experiments. Chemically interesting trends are observed for these functions as a function of atomic number Z. It is believed that these ab initio EXAFS functions can be used in EXAFS data analysis to provide accurate structural (interatomic distances) and chemical (type and number of neighboring atoms, Debye-Waller factors) information.

Introduction

The phenomenon of EXAFS refers to the oscillatory modulation of the X-ray absorption coefficient as a function of X-ray photon energy beyond the absorption edge. The existence of such an extended fine structure has been known and treated theoretically in the 1930s by Kronig.[1] Recent developments[2-21] initiated by the work of Sayers, Stern, and Lytle[2-5] have led to the recognition of the structural content of this technique. At the same time, the availability of synchrotron radiation has greatly improved the speed of data acquisition and S/N by a factor of $\sim 10^5$ over conventional X-ray sources.[11-13] Such developments have gradually established EXAFS as a practical structural tool.

It is now generally accepted that the EXAFS phenomenon is due to a final state interference effect involving scattering of the outgoing photoelectron from the neighboring atoms. This causes an oscillatory behavior of the absorption rate. For reasonable high energy and moderate thermal vibrations, the modulation of the absorption coefficient, normalized to the "background" absorption (μ_0), can be described in terms of the scattering amplitude from the neighboring atom $F(k)$ and the phase shift function $\phi(k)$ which consists of contribution from the absorbing atom and the neighboring atom. If these functions are known, it should be possible to deduce structural information about the local environment of the absorber.

Two major approaches of data analysis have since been developed: the Fourier transform[2-8] and the curve-fitting techniques.[14-21] Both of these methods require a detailed knowledge of the amplitude and phase functions for the determination of chemical information such as coordination number, Debye-Waller factor, and interatomic distances through the assumptions of amplitude and phase transferabilities. These latter hypotheses, which greatly enhance the chemical content of EXAFS spectroscopy, have been demonstrated previously.[4,10,17,21]

Experimentally the amplitude and phase functions can be obtained from the EXAFS spectra of model compounds[2-5,9-11,14,19-21] However, it is often possible to obtain only the product (vide infra) $F_b(k)e^{-2\sigma^2k^2}e^{-2r/\lambda}$ (assuming N is known) for each type of scatterer B and the combined phase $\phi_{ab}(k)$ for each pair of atoms AB (assuming r is known) from experimental data. The extraction of amplitude function $F_b(k)$ alone requires knowledge of the Debye-Waller factor σ (from a separate study or from temperature-dependent measurements) and the electron mean free path λ whereas the separation of the total phase shift ϕ_{ab} into individual phases ϕ_a (due to the absorber A) and ϕ_b (due to the backscatterer B) can only be achieved by measuring the phase shifts of various combinations of pairs of atoms and arbitrarily defining ϕ_a or ϕ_b for one atom.[22]

To avoid the tedious task of searching, measuring, and analyzing model compounds, it is clearly desirable to calculate the amplitude $F(k)$ and the individual phase shifts $\phi_a(k)$ and $\phi_b(k)$ from first principle. With an accurate method, this not only represents a major saving in time and effort, but also greatly reduces the danger of introducing experimental errors from the analyses of model compounds.[15-20]

We have calculated the amplitude and phase functions of nearly half of the elements in the periodic table using an electron-atom scattering theory recently introduced by Lee and Beni.[8] In this paper, we tabulate and plot our results as a function of atomic number Z such that the intermediate elements can readily be interpolated. We have also tested some of these functions in EXAFS data analysis with favorable results.[15-20] Chemically interesting trends can be observed from these plots which either help clarify questions in EXAFS spectroscopy or caution ways of interpreting EXAFS data. The use of these theoretical functions in conjunction with Fourier transform, curve fitting, or a combination of both in EXAFS data analyses has been proven to be highly valuable, especially for complex multiatom, multidistance systems.[16,18-20]

EXAFS of K and L Edges

For the excitation of a s level (K or L_I edge) the absorption coefficient normalized to a smooth background μ_0 can be described by

$$\chi(k) = \frac{\mu - \mu_0}{\mu_0} = \sum_j 3\cos^2\theta_j N_j F_j(k) e^{-2\sigma_j^2k^2}\, e^{-2r_j/\lambda} \frac{\sin(2kr_j + \phi_j(k))}{kr_j^2} \tag{1}$$

where $F_j(k)$ is the backscattering amplitude from each of the N_j neighboring atoms of the jth type with a Debye-Waller factor of σ_j (to account for thermal vibration and static disorder—viz., nonequivalent distances) and at a distance r_j away. The jth neighbor makes an angle θ_j with the polarization vector of the X-ray and the factor $3\cos^2\theta_j$ averages to 1 for polycrystalline samples. $\phi_j(k)$ is the total phase shift experienced by the photoelectron and is given by

$$\phi(k) = \phi_a^{\,l=1}(k) + \phi_b(k) - \pi \tag{2}$$

where ϕ_b is the phase of the backscattering amplitude from the neighbor and $\phi_a{}^l$ equals $2\delta_l'$ where δ_l' is the l phase shift due to the central atom.[8] The term $e^{-2r_j/\lambda}$ is due to inelastic

0002-7863/79/1501-2815$01.00/0

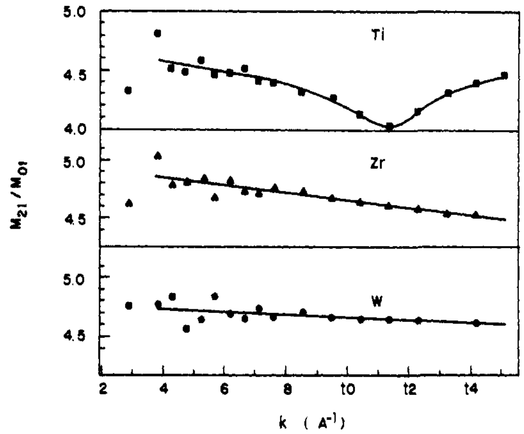

Figure 1. The ratio of the radial dipole matrix elements M_{21}/M_{01} (where M_{21} and M_{01} correspond to the $l = 1$ initial atomic state and the $l = 2$ and $l = 0$ final states, respectively) as a function of electron wave vector k for Ti, Zr, and W.

(scattering) losses with λ being the electron mean free path. Finally k refers to the photoelectron wave vector which is defined as

$$k = \sqrt{\frac{2m}{\hbar^2}(E - E_0)} \qquad (3)$$

where E is the photon energy and E_0 is the energy threshold of the absorption edge. It should also be noted that, while the backscattering amplitude is a function of the scatterer only, the phase shift depends upon both the absorber (central atom) and the backscatterer (neighboring atom).

The description of EXAFS from exciting a p level ($L_{\text{II,III}}$ spectra) is complicated by the fact that the initial p state can go to a final state of s or d symmetry. Instead of the single term in eq 1 we have three terms (eq 4) in which the central atom phase ϕ_a is given by $2\delta_2'$, $2\delta_0'$, and $\delta_0' + \delta_2'$ where δ_l' is the phase shift of an outgoing wave with angular momentum l.[7,23]

$$\chi(k) = \sum_j \frac{N_j F_j(k)}{k r_j^2} e^{-2\sigma_j^2 k^2} e^{-2r_j/\lambda} \times \{\tfrac{1}{2}(1 + 3\cos^2\theta_j)|M_{21}|^2 \sin(2kr_j + \phi_{2j}) + \tfrac{1}{2}|M_{01}|^2 \sin(2kr_j + \phi_{0j}) + M_{01}M_{21}(1 - 3\cos^2\theta_j)\sin(2kr_j + \phi_{02j})\} \times (|M_{21}|^2 + \tfrac{1}{2}|M_{01}|^2)^{-1} \qquad (4)$$

The phase functions for the jth atom are

$$\phi_2 = \phi_a{}^{l=2} + \phi_b \qquad (5a)$$

$$\phi_0 = \phi_a{}^{l=0} + \phi_b \qquad (5b)$$

$$\phi_{02} = \tfrac{1}{2}(\phi_a{}^{l=2} + \phi_a{}^{l=0}) + \phi_b \qquad (5c)$$

Note that in comparison with the K edge or L_{I} edge phase given by eq 2 *the additional factor of π is absent* in eq 5. This is because the π factor has been introduced to take care of an overall minus sign which is absent for $L_{\text{II,III}}$ edge (viz., $\chi(k)$ has a $(-1)^l$ factor where l is the angular momentum of the initial state). The matrix elements M_{01} and M_{21} are the radial dipole matrix elements between the 2p ($l = 1$) atomic wave function and the $l = 2$ and $l = 0$ final states.

For polycrystalline samples the cross term involving $\delta_0' + \delta_2'$ (i.e., the third term in braces in eq 4) vanishes by angular averaging. We are still left with a complicated expression which requires two sets of central atom phase shifts and the ratio between the dipole matrix elements. In our calculation of the phase shift (to be discussed later) we calculate the final state wave function of angular momentum l as an intermediate step. It is straightforward to compute the matrix elements M_{21} and M_{01}.[24] The ratio M_{21}/M_{01} is plotted in Figure 1 as a function of photoelectron momentum k for Ti, Zr, and W. We see that the ratio is of the order of 5 and is relatively independent of k. For light atoms, however, M_{21}/M_{01} shows some k dependence and can vary by as much as a factor of 2 as in, for example, chlorine. From eq 4 we see that transitions to the d final state are favored by a factor of 50. Thus for all practical purposes M_{01} can be ignored and the $L_{\text{II,III}}$ edge can be analyzed in the same way as K and L_{I} edges with the use of the $l = 2$ phase shift given by eq 5a in place of eq 2.

It is interesting to note that the calculated ratio is in excellent agreement with the value $M_{01}/M_{21} = 0.2 \pm 0.06$ obtained by Heald and Stern[23] from the angular dependence of the tungsten L_{III} edge spectrum. The physical reason that M_{01} is smaller is that the $l = 0$ final state must be orthogonal to the 1s core state and therefore is much more rapidly oscillatory than the $l = 2$ final state in the region of the 2p wave function. It should also be mentioned that Lytle, Sayers, and Stern[25] have observed sidebands in the Fourier transform spectrum in the gold L edge and interpreted them as arising from the $l = 0$ final states. The smallness of ratio M_{01}/M_{21} means that the $l = 0$ contribution is practically unobservable and that the sideband is more properly interpreted as arising from the complicated structure in the amplitude and phase functions for heavy atoms (vide infra).

Methods

The ab initio EXAFS amplitude and phase functions presented in this work were calculated with the electron-atom scattering theory originally developed by Lee and Beni.[8] Basically the theory involves the construction of an effective complex scattering potential that adequately accounts for the exchange and correlation effects caused by the electrons in the atom using a modified Thomas-Fermi approach which amounts to replacing the atom by an electron gas with spatially varying density and calculating the self-energy using the plasmon pole approximation. Specifically, the method amounts to first calculating the spatial dependence of the charge density from Hartree-Fock wave functions (vide infra). From this the local Fermi energy and the local momentum can be obtained by using the Thomas-Fermi description of an atom. Then a complex potential is constructed which depends on the kinetic energy of the incoming electron. This complex potential is added to the electrostatic potential to yield the complex phase shifts. This scheme, when applied to the electron-atom scattering problem, gives the backscattering amplitude $F_b(k)$ and the backscattering phase shift $\phi_b(k)$ for the scatterer and the central atom phase shift $\phi_a{}'(k)$ for the absorber in EXAFS spectroscopy. The results for nearly half of the elements in the periodic table with atomic number $Z < 86$ are tabulated in Tables I-VIII.

Tables I-III were calculated using Clementi-Roetti wave functions.[26a] The central atom phase shifts $\phi_a{}'(k)$ were obtained using the unscreened $Z + 1$ ion approximation[8] which amounts to using the $Z + 1$ atomic wave function with one outer (valence) electron missing. The latter was chosen as a compromise for a screened $Z + 1$ atom (completely relaxed case) at low kinetic energy and an unscreened Z ion (completely unrelaxed) at high kinetic energy. These phase shifts have previously been parametrized and published.[17] We have extended these calculations to heavier atoms. We find it more convenient to use the Herman-Skillman wave functions.[26b] Furthermore, for heavier atoms the backscattering amplitude and phase functions cannot be parametrized by simple analytical functions. These more recent results are tabulated in Tables IV-VIII. For the central atom phase shifts the Z ion with one core electron (1s or 2s) missing was used. In all backscattering amplitude (Tables I and IV) and phase (Tables

Table I. Backscattering Amplitudes $F(k)$ in Å vs. Photoelectron Wave Vector k in $Å^{-1}$, Calculated Using Clementi-Roetti Wave Functions

Z	CHEM	k=3.7795	4.2519	4.7243	5.1967	5.6692	6.1416	6.6140	7.0865	7.5589
		8.5038	9.4486	10.3935	11.3384	12.2832	13.2281	14.1729	15.1178	
6	C	0.5063	0.3566	0.2800	0.2430	0.2099	0.1719	0.1430	0.1325	0.1182
		0.0839	0.0712	0.0562	0.0481	0.0397	0.0349	0.0297	0.0267	
8	O	0.7041	0.5781	0.4629	0.3909	0.3248	0.2661	0.2205	0.1913	0.1700
		0.1256	0.1016	0.0814	0.0674	0.0563	0.0489	0.0416	0.0365	
9	F	0.7175	0.6275	0.5294	0.4503	0.3924	0.3273	0.2733	0.2349	0.2038
		0.1532	0.1204	0.0956	0.0792	0.0652	0.0566	0.0481	0.0423	
11	NA	0.6630	0.6007	0.5436	0.4669	0.4310	0.3905	0.3482	0.3023	0.2657
		0.2028	0.1610	0.1263	0.1014	0.0864	0.0715	0.0629	0.0569	
15	P	0.7829	0.7034	0.6517	0.6112	0.5533	0.4806	0.4471	0.4164	0.3671
		0.2938	0.2344	0.1874	0.1571	0.1295	0.1089	0.0939	0.0845	
16	S	0.8140	0.8173	0.7569	0.6523	0.5843	0.5505	0.5075	0.4508	0.3936
		0.3283	0.2608	0.2151	0.1731	0.1459	0.1191	0.1016	0.0854	
17	CL	0.8269	0.8413	0.8188	0.7130	0.6344	0.5755	0.5391	0.4938	0.4361
		0.3475	0.2864	0.2289	0.1901	0.1580	0.1330	0.1100	0.0954	
20	CA	0.6478	0.8064	0.8361	0.7698	0.7051	0.6457	0.5971	0.5404	0.4972
		0.3981	0.3317	0.2776	0.2160	0.1910	0.1630	0.1359	0.1146	
22	TI	0.6225	0.7179	0.7580	0.8075	0.8073	0.7404	0.6822	0.6198	0.5537
		0.4707	0.3844	0.3378	0.2653	0.2197	0.1905	0.1587	0.1391	
24	CR	0.4569	0.5482	0.6666	0.7161	0.7604	0.7668	0.7479	0.6865	0.6354
		0.5288	0.4438	0.3661	0.3089	0.2541	0.2195	0.1863	0.1623	
26	FE	0.3625	0.4285	0.5148	0.5849	0.6800	0.7274	0.7201	0.6942	0.6615
		0.5798	0.4949	0.4189	0.3474	0.2902	0.2451	0.2086	0.1768	
29	CU	0.2757	0.2577	0.3559	0.4352	0.5124	0.6240	0.6680	0.6723	0.6682
		0.6325	0.5587	0.4846	0.4113	0.3480	0.2951	0.2513	0.2178	
32	GE	0.3062	0.2491	0.2677	0.3006	0.3833	0.4995	0.5529	0.5724	0.5982
		0.6124	0.5788	0.5249	0.4674	0.3988	0.3458	0.2934	0.2543	
35	BR	0.3836	0.3144	0.2785	0.2894	0.3386	0.4210	0.5020	0.5485	0.5694
		0.6120	0.5832	0.5513	0.4975	0.4456	0.3826	0.3362	0.2899	

Table II. Backscattering Phase Shifts $\phi_b(k)$ in Radian vs. Photoelectron Wave Vector k in $Å^{-1}$, Calculated Using Clementi-Roetti Wave Functions

Z	CHEM	k=3.7795	4.2519	4.7243	5.1967	5.6692	6.1416	6.6140	7.0865	7.5589
		8.5038	9.4486	10.3935	11.3384	12.2832	13.2281	14.1729	15.1178	
6	C	0.0481	-0.0992	-0.3146	-0.5489	-0.7327	-0.9119	-1.0949	-1.2448	-1.3145
		-1.6305	-1.8127	-2.0773	-2.2421	-2.4449	-2.5762	-2.7436	-2.8657	
8	O	0.5056	0.4555	0.3436	0.1858	0.0530	-0.0643	-0.1986	-0.3627	-0.5035
		-0.7327	-0.9763	-1.1969	-1.4081	-1.6035	-1.7800	-1.9252	-2.0925	
9	F	0.6436	0.5801	0.5072	0.3723	0.2630	0.1815	0.0750	-0.0616	-0.1872
		-0.4056	-0.6354	-0.8457	-1.0587	-1.2427	-1.4357	-1.5878	-1.7465	
11	NA	1.4871	1.4189	1.2842	1.1232	1.0379	0.9245	0.8037	0.7278	0.6167
		0.4132	0.1683	-0.0389	-0.2383	-0.3511	-0.4625	-0.8664	-1.0499	
15	P	3.5897	3.4657	3.3259	3.1419	3.0078	2.8527	2.7088	2.5551	2.4108
		2.1811	1.9250	1.7299	1.4634	1.2613	1.0318	0.8387	0.6943	
16	S	3.6618	3.5265	3.4586	3.3502	3.1962	3.0299	2.8992	2.7921	2.6714
		2.4337	2.1703	1.9651	1.7471	1.5259	1.3306	1.1155	0.9559	
17	CL	3.7781	3.6982	3.6428	3.5596	3.4464	3.3174	3.1796	3.0631	2.9656
		2.7275	2.4810	2.2481	2.0427	1.8078	1.6304	1.4153	1.2463	
20	CA	5.5111	5.1885	5.1244	5.0356	4.9437	4.7719	4.6259	4.4780	4.3182
		4.0505	3.7842	3.5296	3.1526	2.9924	2.8367	2.6625	2.4975	
22	TI	5.0578	5.1829	5.0969	5.0310	5.0209	4.9533	4.8189	4.7412	4.6626
		4.3738	4.1297	3.8988	3.6356	3.4189	3.1788	2.9330	2.6651	
24	CR	4.6789	5.0195	5.1303	5.0781	5.0492	5.0313	5.0002	4.9126	4.8156
		4.6585	4.4184	4.2252	3.9968	3.7829	3.5680	3.3656	3.1832	
26	FE	4.6376	5.1013	5.2163	5.1940	5.1656	5.2196	5.1716	5.1143	5.0787
		4.9115	4.7426	4.5374	4.3659	4.1507	3.9500	3.7421	3.5227	
29	CU	4.3259	4.9690	5.3797	5.4192	5.4286	5.4584	5.4798	5.4447	5.3991
		5.3159	5.1710	5.0326	4.8523	4.6898	4.4958	4.3136	4.1174	
32	GE	4.4485	4.9937	5.4287	5.6053	5.6784	5.7439	5.7959	5.7799	5.7404
		5.6405	5.5145	5.3850	5.2535	5.1026	4.9454	4.7666	4.6126	
35	BR	4.6324	5.0076	5.5637	5.9716	6.2120	6.3555	6.3982	6.3956	6.3713
		6.2729	6.1482	5.9926	5.8585	5.7174	5.5499	5.3929	5.2145	

II and V) function calculations, the wave functions were truncated at 1.5 times the covalent radius and a uniform charge density was added to preserve charge neutrality within this radius. For all central atom phase shift (Tables III, VI–VIII) calculations, the Coulomb field was cut off at twice the covalent radius. All calculations were performed on neutral atoms except for a few alkali and alkali-earth elements, which were treated as cations. The difference between various oxidation

Table III. Central Atom Phase Shifts $\phi_a^{l=1}(k)$ in Radian vs. Photoelectron Wave Vector k in Å^{-1}, Calculated Using Clementi-Roetti Wave Functions and the $(Z + 1)$ Ion Approximation

Z	CHEM	k=3.7795	4.2519	4.7243	5.1967	5.6692	6.1416	6.6140	7.0865	7.5589
		8.5038	9.4486	10.3935	11.3384	12.2832	13.2281	14.1729	15.1178	
12	MG	-3.5617	-3.9685	-4.3733	-4.7701	-5.0669	-5.3543	-5.6428	-5.8338	-6.0636
		-6.4312	-6.7567	-7.0415	-7.2993	-7.5158	-7.7085	-7.8942	-8.0626	
14	SI	-2.3921	-2.9872	-3.4091	-3.7521	-4.0891	-4.4444	-4.7279	-4.9464	-5.1959
		-5.6061	-5.9793	-6.2763	-6.5604	-6.8066	-7.0308	-7.2375	-7.4235	
16	S	-1.5587	-2.1042	-2.5678	-2.9541	-3.2763	-3.6236	-3.9540	-4.2141	-4.4305
		-4.9052	-5.2781	-5.6170	-5.9076	-6.1779	-6.4301	-6.6363	-6.8490	
21	SC	1.1795	0.6230	0.1224	-0.3994	-0.7927	-1.1724	-1.5605	-1.8614	-2.1806
		-2.7211	-3.2072	-3.6470	-4.0255	-4.3628	-4.6688	-4.9459	-5.2051	
23	V	1.5350	0.9061	0.3468	-0.0757	-0.4409	-0.8628	-1.1871	-1.4872	-1.8112
		-2.3372	-2.8357	-3.2666	-3.6301	-3.9812	-4.2905	-4.5668	-4.8298	
26	FE	2.0856	1.4838	0.9136	0.4869	0.1332	-0.2651	-0.6151	-0.9053	-1.2124
		-1.7320	-2.2309	-2.6475	-3.0347	-3.3885	-3.7033	-3.9952	-4.2651	
29	CU	2.5785	1.9474	1.4064	1.0160	0.6236	0.2288	-0.0929	-0.3817	-0.6966
		-1.2194	-1.7082	-2.1233	-2.5115	-2.8684	-3.1826	-3.4880	-3.7629	
32	GE	3.2853	2.6446	2.1916	1.7551	1.3016	0.9493	0.6306	0.2722	-0.0379
		-0.5737	-1.0568	-1.5087	-1.8904	-2.2483	-2.5956	-2.8984	-3.1768	
35	BR	4.2011	3.5744	3.0770	2.6538	2.2224	1.8180	1.4768	1.1480	0.8028
		0.2540	-0.2749	-0.7220	-1.1320	-1.5120	-1.8640	-2.1812	-2.4812	
40	ZR	7.1080	6.4124	5.8533	5.2006	4.7033	4.2814	3.8093	3.4067	3.0375
		2.3621	1.7442	1.1970	0.7108	0.2704	-0.1353	-0.5099	-0.8646	
45	RH	6.4865	6.0246	5.5155	4.9999	4.5687	4.2071	3.8180	3.4570	3.1318
		2.5292	1.9858	1.4785	1.0327	0.6200	0.2359	-0.1138	-0.4461	
52	TE	9.1879	8.5796	8.0058	7.4207	6.9617	6.5146	6.0481	5.6693	5.2845
		4.6178	3.9937	3.4310	2.9335	2.4710	2.0384	1.6423	1.2821	

Table IV. Backscattering Amplitudes $F(k)$ in Å vs. Photoelectron Wave Vector k in Å^{-1}, Calculated Using Herman-Skillman Wave Functions

Z	CHEM	k=3.7795	4.2519	4.7243	5.1967	5.6692	6.1416	6.6140	7.0865	7.5589
		8.5038	9.4486	10.3935	11.3384	12.2832	13.2281	14.1729	15.1178	
14	SI	0.7326	0.7068	0.6358	0.5533	0.5208	0.4815	0.4223	0.3760	0.3439
		0.2745	0.2215	0.1771	0.1466	0.1183	0.1004	0.0836	0.0727	
17	CL	0.7740	0.8130	0.7927	0.7050	0.6256	0.5710	0.5316	0.4883	0.4323
		0.3441	0.2857	0.2288	0.1905	0.1597	0.1338	0.1111	0.0960	
20	CA	0.6805	0.7672	0.8078	0.7555	0.7002	0.6389	0.5916	0.5387	0.4937
		0.3976	0.3310	0.2771	0.2213	0.1915	0.1618	0.1350	0.1135	
40	ZR	0.6463	0.5510	0.4291	0.3454	0.3190	0.3513	0.4217	0.4807	0.5192
		0.5842	0.5784	0.5596	0.5253	0.4791	0.4349	0.3904	0.3366	
42	MO	0.7500	0.6977	0.5944	0.4233	0.3582	0.3596	0.3894	0.4570	0.5172
		0.5779	0.5960	0.5729	0.5452	0.5019	0.4509	0.4085	0.3668	
44	RU	0.8645	0.7911	0.7219	0.5553	0.4243	0.3835	0.3894	0.4305	0.4903
		0.5732	0.5976	0.5900	0.5623	0.5218	0.4755	0.4239	0.3837	
46	PD	0.9115	0.8554	0.7922	0.6655	0.5083	0.4197	0.3822	0.3984	0.4530
		0.5519	0.5944	0.5994	0.5813	0.5413	0.4974	0.4470	0.4068	
47	AG	0.9143	0.8729	0.8121	0.6993	0.5558	0.4354	0.3745	0.3895	0.4358
		0.5330	0.5923	0.6008	0.5881	0.5517	0.5066	0.4616	0.4198	
50	SN	1.1146	1.0135	0.8812	0.7798	0.6296	0.4939	0.4107	0.4014	0.4261
		0.5174	0.5849	0.6142	0.6031	0.5789	0.5380	0.4940	0.4395	
53	I	1.1468	1.0382	0.9153	0.8085	0.6808	0.5630	0.4660	0.4215	0.4238
		0.5065	0.5883	0.6233	0.6313	0.6063	0.5680	0.5190	0.4749	
57	LA	0.6221	0.7004	0.7250	0.7630	0.6704	0.5967	0.5238	0.4512	0.4503
		0.5067	0.5901	0.6420	0.6381	0.6242	0.6089	0.5548	0.5164	
58	CE	0.6161	0.6850	0.6812	0.7354	0.6726	0.5940	0.5272	0.4443	0.4224
		0.4573	0.5524	0.6158	0.6300	0.6188	0.6083	0.5663	0.5188	
65	TB	0.3467	0.4390	0.4390	0.5228	0.5789	0.5519	0.5369	0.4821	0.4263
		0.3606	0.3836	0.4589	0.5367	0.5707	0.6010	0.5999	0.5772	
70	YB	0.2904	0.3517	0.3241	0.3897	0.4710	0.4782	0.4918	0.4765	0.4360
		0.3677	0.3169	0.3367	0.4202	0.4868	0.5316	0.5826	0.5791	
74	W	0.3196	0.2523	0.1939	0.1996	0.2903	0.4000	0.4404	0.4525	0.4603
		0.3985	0.3366	0.3169	0.3750	0.4554	0.5122	0.5417	0.5693	
76	OS	0.4614	0.3804	0.2549	0.1401	0.1989	0.2965	0.3971	0.4521	0.4538
		0.4310	0.3461	0.3195	0.3555	0.4355	0.4984	0.5467	0.5628	
78	PT	0.5711	0.5106	0.3803	0.1694	0.0819	0.1982	0.3370	0.4127	0.4430
		0.4431	0.3649	0.3193	0.3409	0.4138	0.4798	0.5289	0.5488	
80	HG	0.6538	0.5718	0.4872	0.3073	0.0806	0.1015	0.2527	0.3666	0.4265
		0.4496	0.3826	0.3250	0.3269	0.3914	0.4466	0.5088	0.5499	
82	PB	0.8557	0.7215	0.5926	0.3856	0.1469	0.0945	0.2350	0.3655	0.4384
		0.4701	0.4067	0.3415	0.3295	0.3866	0.4381	0.4958	0.5415	

Table V. Backscattering Phase Shifts $\phi_b(k)$ in Radian vs. Photoelectron Wave Vector k in Å^{-1}, Calculated Using Herman-Skillman Wave Functions

Z	CHEM	k=3.7795	4.2519	4.7243	5.1967	5.6692	6.1416	6.6140	7.0865	7.5589
		8.5038	9.4486	10.3935	11.3384	12.2832	13.2281	14.1729	15.1178	
14	SI	2.8451	2.7102	2.5684	2.4237	2.2930	2.1695	2.0314	1.8893	1.7979
		1.5790	1.3425	1.1418	0.9229	0.7272	0.5244	0.3251	0.1337	
17	CL	3.5339	3.4935	3.4518	3.3727	3.2504	3.1405	3.0158	2.9084	2.8179
		2.5775	2.3437	2.1201	1.9182	1.6835	1.5147	1.3126	1.1424	
20	CA	4.9368	4.9506	4.9006	4.8040	4.7095	4.5616	4.4313	4.2976	4.1491
		3.8851	3.6277	3.3828	3.0205	2.8617	2.7022	2.5257	2.3615	
40	ZR	5.5087	5.6976	5.9968	6.3248	6.7537	7.1845	7.3301	7.3862	7.3997
		7.3259	7.2062	7.0627	6.8848	6.7291	6.5750	6.4172	6.2162	
42	MO	5.3241	5.6417	5.9025	6.2277	6.5820	6.9913	7.3814	7.5168	7.5415
		7.5779	7.4839	7.3453	7.1972	7.0307	6.8815	6.7131	6.5743	
44	RU	5.1521	5.5560	5.8075	6.1610	6.4952	6.8481	7.2943	7.5823	7.6837
		7.7764	7.7103	7.6053	7.4610	7.3223	7.1668	7.0090	6.8538	
46	PD	4.9785	5.4527	5.7202	6.0619	6.3308	6.6559	7.1120	7.4861	7.6767
		7.8956	7.8671	7.8056	7.6815	7.5570	7.4254	7.2556	7.1135	
47	AG	4.9498	5.4256	5.7322	6.0104	6.2758	6.5895	7.0201	7.4073	7.6789
		7.9364	7.9624	7.8971	7.7941	7.6706	7.5470	7.3844	7.2409	
50	SN	6.2323	6.5485	6.7944	6.9256	7.0671	7.3134	7.5998	7.9268	8.2718
		8.5524	8.6258	8.5639	8.4687	8.3487	8.2004	8.0240	7.8928	
53	I	7.2328	7.4433	7.5482	7.6736	7.7480	7.9092	8.1375	8.3787	8.6663
		9.0611	9.1503	9.1388	9.0401	8.9299	8.8010	8.6309	8.4567	
57	LA	9.1054	9.1140	9.0879	9.0990	9.0917	9.1506	9.2783	9.4672	9.6694
		10.0405	10.1739	10.1463	10.0304	9.9063	9.7864	9.6034	9.4633	
58	CE	8.8314	8.8587	8.7713	8.8249	8.8322	8.8543	8.9636	9.1388	9.3441
		9.7813	9.9848	9.9920	9.9276	9.8101	9.7087	9.5561	9.4087	
65	TB	8.9896	9.0186	8.8981	8.8092	8.7686	8.7275	8.7431	8.7896	8.8404
		9.2244	9.6925	9.9728	10.0507	10.0328	9.9813	9.9134	9.8120	
70	YB	9.1561	9.1654	9.1020	8.9196	8.8057	8.7093	8.6750	8.6419	8.6522
		8.8262	9.2384	9.7232	9.9597	10.0334	10.0505	10.0326	9.9615	
74	W	10.8847	10.8005	10.3731	9.7269	9.3337	9.2044	9.1181	9.0581	9.0780
		9.1798	9.5185	9.9579	10.2952	10.4195	10.4622	10.4376	10.3847	
76	OS	10.9741	11.2710	11.3216	10.2771	9.5414	9.2519	9.1696	9.1667	9.1447
		9.2602	9.5576	9.9875	10.3635	10.5346	10.6037	10.5956	10.5386	
78	PT	11.1468	11.5015	11.6393	11.5297	10.1376	9.3255	9.2371	9.2168	9.1978
		9.3455	9.6205	10.0458	10.4390	10.6673	10.7535	10.7584	10.7178	
80	HG	11.5236	11.6950	11.8774	12.0838	11.8658	9.2967	9.2339	9.3059	9.3491
		9.4588	9.7259	10.1046	10.4877	10.7982	10.9296	10.9448	10.9055	
82	PB	12.3853	12.5708	12.7450	12.9479	13.2543	8.9454	9.4699	9.6543	9.7369
		9.8628	10.1082	10.4315	10.8212	11.1250	11.2779	11.2993	11.2529	

states, though small but significant, can be compensated by changing the threshold energy (vide infra). The valence electronic configuration for the three transition metal series were $3d^{Z-20}4s^2$, $4d^{Z-37}5s^1$, and $5d^{Z-70}6s^2$. Again, the difference between various electronic configurations can largely be compensated by E_0 variation. We also should point out that the Herman-Skillman wave functions are inadequate for heavy atoms (beyond the rare earths, for instance) because of relativistic corrections. We have used relativistic wave functions for tungsten and the result is shown in a later section. We find, however, that the difference is sufficiently small to justify the use of the more readily available nonrelativistic Herman-Skillman wave functions for all elements.

Results and Discussion

In this paper, we report ab initio theoretical EXAFS functions in the range of $k \simeq 4$-15 Å^{-1}. The truncation at low k value ($k \simeq 4$ Å^{-1}) is due to the fact that the theory is less reliable for $k \lesssim 4$ Å^{-1} as a result of inadequate treatment of valence electrons, particularly for light atoms with $Z \lesssim 9$ where the energy of the valence electrons is a substantial portion of that of the core electrons. Furthermore, other physical phenomena such as multiple scattering may become important at low k values. At high k values ($k \gtrsim 15$ Å^{-1}), the EXAFS signal is generally attenuated substantially by Debye-Waller factor.

Throughout this paper, we chose to use the "experimental" unit of ångstroms for the amplitude function $F(k)$ (cf. Tables I and IV), radian for the phase functions $\phi(k)$ (cf. Tables II, III, V-VIII), and Å^{-1} for the electron wave vector k. It should also be noted that the functions $F(k)$, $\phi_b(k)$, and $\phi_a'(k)$ reported in this paper are equivalent to the functions $f(\pi,k)$, $\theta(k)$, and $2\delta_l'(k)$ (in atomic units) used in Lee and Beni's paper.[8] Furthermore, if we have an absorbing atom A and a backscattering atom B, we denote the phase function by ϕ_{ab} which is given by

$$\phi_{ab}(k) = \phi_a'(k) + \phi_b(k) - \pi,\ l = 1 \text{ for } K \text{ and } L_{\rm I} \text{ edges} \tag{6a}$$

$$\phi_{ab}(k) = \phi_a'(k) + \phi_b(k),\ l = 2,0 \text{ for } L_{\rm II,III} \text{ edges} \tag{6b}$$

where ϕ_a' is the phase shift of the central atom A and ϕ_b is the phase shift of the neighboring atom B.

A detailed comparison of Tables I-III (Clementi-Roetti[26a] wave functions) with Tables IV-VIII (Herman-Skillman[26b] wave functions) revealed that the two sets of results agree quite well with the exception of central atom (absorber) phase shifts. A comparison of Table III with the corresponding Table VII showed that the $(Z + 1)$ approximation in the former case results in more positive phase shifts. The difference (ca. 0.7-0.2 rad), however, decreases with increasing k values and therefore can be substantially removed by changing the energy threshold

Table VI. Central Atom Phase Shifts $\phi_a{}^{l=0}(k)$ in Radian vs. Photoelectron Wave Vector k in Å^{-1}, Calculated Using Herman-Skillman Wave Functions

Z	CHEM									
		k=3.7795	4.2519	4.7243	5.1967	5.6692	6.1416	6.6140	7.0865	7.5589
		8.5038	9.4486	10.3935	11.3384	12.2832	13.2281	14.1729	15.1178	
11	NA+	-5.6231	-6.3933	-6.8848	-7.3767	-7.8876	-8.2287	-8.6431	-8.9622	-9.2652
		-9.8182	-10.3291	-10.7726	-11.1661	-11.5138	-11.8216	-12.1021	-12.3581	
12	MG++	-3.8448	-4.6324	-5.3798	-5.8169	-6.3347	-6.8851	-7.2518	-7.6238	-8.0287
		-8.6331	-9.1791	-9.7016	-10.1483	-10.5207	-10.8800	-11.2092	-11.5071	
14	SI	-5.1257	-5.7878	-6.3136	-6.7332	-7.1618	-7.5758	-7.9339	-8.2163	-8.5254
		-9.0594	-9.5388	-9.9391	-10.3355	-10.6638	-10.9752	-11.2682	-11.5251	
17	CL	-3.9386	-4.5306	-5.0641	-5.5371	-5.9210	-6.3182	-6.7155	-7.0543	-7.3263
		-7.9082	-8.3831	-8.8327	-9.2170	-9.5822	-9.9003	-10.2143	-10.4905	
19	K+	-0.8143	-1.6909	-2.2709	-2.9487	-3.4504	-3.9979	-4.4169	-4.8718	-5.2530
		-5.9536	-6.5740	-7.1175	-7.5960	-8.0316	-8.4189	-8.7911	-9.1260	
20	CA++	0.6406	-0.0014	-0.8699	-1.4697	-2.0743	-2.6683	-3.1234	-3.6604	-4.0268
		-4.8218	-5.5110	-6.1175	-6.6567	-7.1396	-7.5766	-7.9730	-8.3377	
20	CA	-1.6038	-2.3361	-2.8941	-3.4800	-3.9310	-4.4009	-4.8048	-5.1989	-5.5518
		-6.2042	-6.7698	-7.2768	-7.7304	-8.1389	-8.5121	-8.8554	-9.1691	
22	TI	-1.3496	-2.0813	-2.6117	-3.1165	-3.6305	-4.0214	-4.3987	-4.8077	-5.1324
		-5.7680	-6.3163	-6.8133	-7.2728	-7.6814	-8.0480	-8.3895	-8.7136	
26	FE	-0.5981	-1.2789	-1.8973	-2.3640	-2.7732	-3.2195	-3.6079	-3.9363	-4.2863
		-4.9006	-5.4475	-5.9420	-6.3928	-6.7960	-7.1690	-7.5194	-7.8358	
28	NI	-0.2909	-0.9459	-1.5472	-2.0204	-2.4204	-2.8508	-3.2421	-3.5710	-3.9074
		-4.5158	-5.0653	-5.5374	-5.9978	-6.4019	-6.7785	-7.1283	-7.4465	
32	GE	0.8703	0.2092	-0.2978	-0.8170	-1.3128	-1.7093	-2.0806	-2.4920	-2.8277
		-3.4527	-4.0051	-4.5191	-4.9725	-5.3879	-5.7904	-6.1490	-6.4830	
35	BR	1.7659	1.1103	0.5794	0.0977	-0.4215	-0.8458	-1.2233	-1.6066	-1.9886
		-2.6082	-3.2051	-3.7131	-4.1773	-4.6187	-5.0200	-5.3906	-5.7394	
40	ZR	3.8309	3.1251	2.5669	1.9563	1.4417	1.0104	0.5316	0.1307	-0.2532
		-0.9471	-1.5886	-2.1614	-2.6682	-3.1331	-3.5692	-3.9683	-4.3512	
42	MO	4.2333	3.4817	2.8584	2.3604	1.8328	1.3441	0.9345	0.5199	0.1211
		-0.5622	-1.1870	-1.7663	-2.2750	-2.7419	-3.1818	-3.5866	-3.9524	
44	RU	4.5455	3.8317	3.1836	2.6907	2.1956	1.6875	1.2868	0.9049	0.5003
		-0.1749	-0.8243	-1.3863	-1.8955	-2.3768	-2.8095	-3.2053	-3.5863	
46	PD	4.8624	4.1300	3.5221	3.0478	2.5299	2.0388	1.6580	1.2552	0.8468
		0.1802	-0.4482	-1.0313	-1.5420	-2.0109	-2.4527	-2.8626	-3.2327	
50	SN	6.1712	5.5288	4.8544	4.2728	3.8081	3.2835	2.8175	2.4217	1.9980
		1.3042	0.6382	0.0332	-0.5017	-0.9909	-1.4469	-1.8849	-2.2776	
53	I	6.9861	6.3488	5.6996	5.0999	4.5908	4.0966	3.6020	3.1848	2.7917
		2.0548	1.3868	0.7883	0.2369	-0.2833	-0.7488	-1.1859	-1.5902	
57	LA	8.9217	8.2145	7.4576	6.8800	6.2577	5.7083	5.2118	4.7188	4.2983
		3.5052	2.7852	2.1321	1.5268	0.9808	0.4739	-0.0014	-0.4375	
58	CE	8.8166	8.1511	7.4003	6.8131	6.2281	5.6672	5.1862	4.6962	4.2806
		3.4880	2.7814	2.1388	1.5480	1.0024	0.5109	0.0419	-0.4007	
64	GD	9.4593	8.8153	8.0828	7.4980	6.9600	6.3999	5.9272	5.4477	5.0296
		4.2472	3.5518	2.9159	2.3326	1.8002	1.3049	0.8393	0.4053	
70	YB	9.7131	9.0941	8.4302	7.8181	7.2945	6.7735	6.3181	5.8661	5.4388
		4.6757	4.0225	3.4051	2.8361	2.3099	1.8207	1.3664	0.9411	
74	W	10.4268	9.6477	9.0202	8.4815	7.9303	7.3854	6.9506	6.5046	6.0647
		5.3324	4.6571	4.0207	3.4588	2.9322	2.4358	1.9818	1.5598	
76	OS	10.6930	9.9356	9.2906	8.7545	8.2274	7.6945	7.2307	6.8067	6.3706
		5.6367	4.9411	4.3220	3.7535	3.2160	2.7260	2.2752	1.8352	
78	PT	10.9689	10.2018	9.5890	9.0822	8.5108	7.9961	7.5602	7.0946	6.6577
		5.9321	5.2571	4.6173	4.0381	3.5196	3.0234	2.5544	2.1299	
80	HG	11.2355	10.5896	9.9143	9.3646	8.8521	8.2996	7.8570	7.4171	6.9807
		6.2308	5.5580	4.9246	4.3319	3.8022	3.3126	2.8496	2.4138	
82	PB	11.9467	11.2913	10.5835	10.0159	9.4675	8.9075	8.4542	7.9969	7.5528
		6.7782	6.0730	5.4323	4.8243	4.2836	3.7834	3.3072	2.8597	

(vide infra). Furthermore, it should be noted that the phase functions are listed and plotted as an increasing function of atomic number Z merely for clarity and for the purpose of facilitating interpolation of the phase shifts of intermediate Z elements. In practice, any phase functions can be modified by $\pm 2n\pi$ where $n = 0, 1, 2, 3, \ldots$, since $\sin(\phi(k) \pm 2n\pi) = \sin(\phi(k))$. With these remarks, we shall now discuss the backscattering amplitude ($F(k)$), the backscattering phase ($\phi_b(k)$), and the central atom phase shifts ($\phi_a(k)$) with the aid of Figures 2–14.

Amplitude. Figures 2a and 2b depict the scattering amplitudes for two main groups 7A and 4A, respectively, whereas Figure 2c shows the amplitude functions of the transition metals Fe, Ru, and Os. It is apparent that as the atomic number Z increases the scattering amplitude at high k values generally increases. More importantly, there are peaks and valleys in the amplitude functions which move to higher k values as Z increases. These amplitude peaks correspond to the resonances of the electron-atom scattering process and can be associated with the $\frac{1}{2}\pi$ crossings of phase shifts with different l values. Figures 3a–d show how these peaks and valleys progress within each series. For light atoms with $Z \lesssim 10$, the amplitude function peaks at the low k region ($\lesssim 3$ Å^{-1}) such that only a monotonically decreasing function is observed. This structureless tail is due to the fact that, when the electron exceeds the binding energy of the deepest shell, the electron is

Table VII. Central Atom Phase Shifts $\phi_a^{l=1}(k)$ in Radian vs. Photoelectron Wave Vector k in Å^{-1}, Calculated Using Herman-Skillman Wave Functions

Z	CHEM	k=3.7795	4.2519	4.7243	5.1967	5.6692	6.1416	6.6140	7.0865	7.5589
		8.5038	9.4486	10.3935	11.3384	12.2832	13.2281	14.1729	15.1178	
6	C	-7.0744	-7.2817	-7.4487	-7.6994	-7.9676	-8.1821	-8.3345	-8.4618	-8.6018
		-8.8888	-9.0707	-9.2798	-9.4242	-9.5691	-9.6967	-9.8045	-9.9151	
8	O	-6.5189	-6.7480	-6.9315	-7.1700	-7.4127	-7.6278	-7.7959	-7.9196	-8.0470
		-8.3582	-8.5693	-8.7617	-8.9497	-9.0839	-9.2360	-9.3545	-9.4670	
9	F	-6.2972	-6.5199	-6.7071	-6.9492	-7.2004	-7.4174	-7.5870	-7.7204	-7.8349
		-8.1329	-8.3485	-8.5462	-8.7425	-8.8804	-9.0351	-9.1566	-9.2720	
11	NA+	-3.2155	-3.8481	-4.2669	-4.6247	-5.0507	-5.2996	-5.6235	-5.8562	-6.0813
		-6.4784	-6.8412	-7.1488	-7.4189	-7.6600	-7.8716	-8.0583	-8.2261	
12	MG++	-1.4390	-2.0405	-2.7238	-3.0884	-3.4938	-3.9705	-4.2603	-4.5530	-4.8926
		-5.3568	-5.7625	-6.1516	-6.4918	-6.7651	-7.0197	-7.2475	-7.4645	
14	SI	-2.8651	-3.4002	-3.8494	-4.1870	-4.5117	-4.8393	-5.1257	-5.3292	-5.5617
		-5.9614	-6.3161	-6.5963	-6.8764	-7.1045	-7.3137	-7.5183	-7.6926	
17	CL	-1.7939	-2.2287	-2.6765	-3.0897	-3.3912	-3.6954	-4.0199	-4.2977	-4.5038
		-4.9602	-5.3250	-5.6685	-5.9513	-6.2241	-6.4524	-6.6771	-6.8757	
19	K+	1.3571	0.6147	0.0905	-0.4883	-0.9257	-1.4047	-1.7551	-2.1531	-2.4673
		-3.0579	-3.5781	-4.0250	-4.4108	-4.7602	-5.0656	-5.3588	-5.6179	
20	CA++	2.9048	2.2965	1.5766	0.9778	0.4902	-0.0731	-0.4507	-0.9338	-1.2464
		-1.9394	-2.5310	-3.0439	-3.4957	-3.8939	-4.2513	-4.5735	-4.8644	
20	CA	0.5733	-0.0952	-0.5599	-1.0552	-1.4490	-1.8348	-2.1860	-2.5083	-2.8093
		-3.3537	-3.8148	-4.2257	-4.5900	-4.9121	-5.2042	-5.4720	-5.7105	
22	TI	0.7928	0.1399	-0.3505	-0.7510	-1.1891	-1.5297	-1.8307	-2.1774	-2.4535
		-2.9774	-3.4271	-3.8348	-4.2071	-4.5351	-4.8252	-5.0924	-5.3461	
26	FE	1.3837	0.8536	0.3077	-0.1080	-0.4466	-0.8114	-1.1523	-1.4268	-1.7096
		-2.2304	-2.6766	-3.0871	-3.4565	-3.7820	-4.0841	-4.3658	-4.6186	
28	NI	1.6350	1.1435	0.6110	0.1706	-0.1425	-0.4901	-0.8352	-1.1129	-1.3810
		-1.8995	-2.3468	-2.7365	-3.1171	-3.4458	-3.7537	-4.0366	-4.2916	
32	GE	2.8531	2.2248	1.7630	1.3573	0.9298	0.5690	0.2700	-0.0767	-0.3758
		-0.8942	-1.3665	-1.7991	-2.1741	-2.5210	-2.8564	-3.1522	-3.4270	
35	BR	3.7269	3.1353	2.6303	2.2422	1.8157	1.4317	1.0971	0.7827	0.4517
		-0.0860	-0.5993	-1.0274	-1.4246	-1.7951	-2.1336	-2.4457	-2.7370	
40	ZR	5.8079	5.1256	4.6373	4.1281	3.6490	3.2773	2.8561	2.4865	2.1632
		1.5447	0.9799	0.4818	0.0414	-0.3642	-0.7440	-1.0869	-1.4163	
42	MO	6.1471	5.5279	4.9250	4.4785	4.0464	3.6009	3.2270	2.8816	2.5219
		1.9237	1.3660	0.8583	0.4160	0.0058	-0.3779	-0.7269	-1.0414	
44	RU	6.4206	5.8617	5.2665	4.7926	4.3806	3.9385	3.5686	3.2431	2.8949
		2.2888	1.7143	1.2250	0.7741	0.3513	-0.0242	-0.3677	-0.6993	
46	PD	6.7635	6.1581	5.5692	5.1463	4.7175	4.2611	3.9233	3.5903	3.2188
		2.6376	2.0726	1.5596	1.1130	0.6981	0.3114	-0.0450	-0.3665	
47	AG	7.4130	7.0555	6.6507	6.3647	6.0790	5.7689	5.5393	5.3076	5.0642
		4.6584	4.2777	3.9214	3.6012	3.3222	3.0718	2.8187	2.6021	
50	SN	8.0817	7.4989	6.9398	6.3880	5.9590	5.5205	5.0864	4.7366	4.3678
		3.7451	3.1433	2.6045	2.1309	1.6957	1.2903	0.9009	0.5570	
53	I	8.9247	8.3161	7.7791	7.2392	6.7528	6.3289	5.8870	5.4941	5.1532
		4.4825	3.8899	3.3529	2.8544	2.3887	1.9751	1.5843	1.2241	
55	CS+	10.3098	9.6092	8.8908	8.3605	7.9268	7.4458	6.9389	6.5101	6.1637
		5.4374	4.8397	4.2264	3.7234	3.2053	2.7855	2.3499	1.9675	
57	LA	10.8567	10.2554	9.5608	9.0124	8.4708	7.9414	7.5065	7.0439	6.6639
		5.9371	5.2814	4.6881	4.1370	3.6430	3.1842	2.7531	2.3596	
58	CE	10.7507	10.1561	9.4991	8.9259	8.4226	7.8903	7.4572	7.0182	6.6274
		5.9071	5.2682	4.6874	4.1510	3.6564	3.2123	2.7865	2.3858	
64	GD	11.3615	10.7710	10.1419	9.5739	9.1174	8.6007	8.1617	7.7395	7.3430
		6.6353	6.0082	5.4315	4.9007	4.4168	3.9662	3.5430	3.1502	
70	YB	11.5744	10.9738	10.4332	9.8476	9.3850	8.9363	8.5022	8.1120	7.7131
		7.0261	6.4381	5.8762	5.3578	4.8803	4.4379	4.0281	3.6442	
74	W	12.2519	11.6107	10.9990	10.4924	10.0398	9.5418	9.1289	8.7431	8.3425
		7.6748	7.0550	6.4830	5.9731	5.4897	5.0400	4.6301	4.2456	
76	OS	12.5102	11.8931	11.2782	10.7721	10.3217	9.8559	9.4097	9.0322	8.6483
		7.9683	7.3377	6.7810	6.2573	5.7681	5.3254	4.9137	4.5123	
78	PT	12.8279	12.1642	11.5505	11.0983	10.6215	10.1311	9.7348	9.3312	8.9200
		8.2696	7.6463	7.0656	6.5410	6.0655	5.6126	5.1879	4.8013	
80	HG	13.0831	12.4816	11.9145	11.3844	10.9332	10.4476	10.0268	9.6428	9.2403
		8.5622	7.9474	7.3650	6.8229	6.3431	5.8984	5.4754	5.0767	
82	PB	13.7859	13.2106	12.6005	12.0451	11.5681	11.0660	10.6298	10.2276	9.8130
		9.1126	8.4636	7.8730	7.3162	6.8247	6.3675	5.9295	5.5188	

sampling mostly the nuclear potential. For elements with $10 \lesssim Z \lesssim 30$, we observe an amplitude envelope whose peak height decreases while its peak position advances in k as Z increases. For elements with $30 \lesssim Z \lesssim 54$, we find one peak and one valley in the amplitude function. A second peak starts to come in from the low k region. Both peaks increase in amplitude and advance in peak position as Z increases. For elements with $57 \lesssim Z \lesssim 71$, both peaks advance in peak position

Table VIII. Central Atom Phase Shifts $\phi_a^{l=2}(k)$ in Radian vs. Photoelectron Wave Vector k in Å^{-1}, Calculated Using Herman-Skillman Wave Functions

Z	CHEM	k=3.7795	4.2519	4.7243	5.1967	5.6692	6.1416	6.6140	7.0865	7.5589
		8.5038	9.4486	10.3935	11.3384	12.2832	13.2281	14.1729	15.1178	
11	NA+	-0.3995	-0.8132	-0.9636	-1.1910	-1.4274	-1.5356	-1.7250	-1.8052	-1.9704
		-2.1820	-2.3796	-2.5390	-2.6900	-2.8270	-2.9523	-3.0639	-3.1649	
12	MG++	1.3366	0.9309	0.4564	0.3056	-0.0218	-0.3142	-0.4408	-0.6764	-0.8554
		-1.1806	-1.4292	-1.6413	-1.8642	-2.0579	-2.2275	-2.3535	-2.4818	
14	SI	-0.7863	-1.0065	-1.2323	-1.3593	-1.4973	-1.6609	-1.7749	-1.8344	-1.9419
		-2.1014	-2.2746	-2.4059	-2.5426	-2.6554	-2.7539	-2.8504	-2.9472	
17	CL	-0.2270	-0.2936	-0.4897	-0.7129	-0.8225	-0.9409	-1.1002	-1.2162	-1.2796
		-1.5121	-1.6571	-1.8275	-1.9597	-2.0875	-2.2033	-2.3084	-2.4182	
19	K+	2.9156	2.5286	2.1377	1.8014	1.5062	1.2084	1.0116	0.7518	0.5703
		0.2063	-0.1042	-0.3633	-0.5900	-0.8017	-0.9859	-1.1670	-1.3169	
20	CA++	4.7443	4.1594	3.7548	3.2475	2.9594	2.5239	2.2975	1.9436	1.7547
		1.2801	0.8908	0.5610	0.2602	0.0020	-0.2311	-0.4373	-0.6244	
20	CA	2.0448	1.6636	1.3692	1.1028	0.8626	0.6594	0.4565	0.2822	0.1137
		-0.1949	-0.4470	-0.6673	-0.8742	-1.0508	-1.2141	-1.3598	-1.4922	
22	TI	2.0353	1.7127	1.3722	1.1717	0.9422	0.7419	0.6008	0.4051	0.2559
		-0.0259	-0.2628	-0.4696	-0.6788	-0.8663	-1.0169	-1.1526	-1.2932	
26	FE	2.2020	1.9926	1.7277	1.4388	1.2717	1.1124	0.9207	0.7721	0.6362
		0.3515	0.1303	-0.0759	-0.2748	-0.4459	-0.6032	-0.7529	-0.8865	
28	NI	2.2964	2.0904	1.8684	1.5675	1.4034	1.2655	1.0768	0.9185	0.8013
		0.5233	0.3003	0.1068	-0.0928	-0.2627	-0.4257	-0.5750	-0.7118	
32	GE	3.4808	3.1522	2.7816	2.5499	2.3530	2.1165	1.9519	1.7749	1.5910
		1.3132	1.0420	0.8017	0.6026	0.4131	0.2241	0.0594	-0.0915	
35	BR	4.2896	4.0442	3.6549	3.3775	3.1748	2.9537	2.7140	2.5398	2.3480
		2.0083	1.7061	1.4580	1.2218	1.0069	0.8098	0.6283	0.4587	
40	ZR	6.3946	6.0007	5.6098	5.3205	4.9774	4.7086	4.4491	4.1646	3.9606
		3.5365	3.1589	2.8311	2.5430	2.2758	2.0247	1.8051	1.5931	
42	MO	6.6133	6.3255	5.9501	5.5844	5.3187	5.0429	4.7477	4.5307	4.2950
		3.8789	3.4912	3.1549	2.8612	2.5850	2.3293	2.1041	1.9009	
44	RU	6.8945	6.5710	6.2631	5.8888	5.5835	5.3282	5.0698	4.8339	4.6216
		4.1896	3.8014	3.4727	3.1599	2.8769	2.6276	2.4024	2.1809	
46	PD	7.1714	6.8840	6.5244	6.1577	5.9111	5.6099	5.3509	5.1543	4.9069
		4.5062	4.1031	3.7560	3.4523	3.1646	2.9073	2.6681	2.4569	
50	SN	8.7603	8.2233	7.8591	7.4918	7.1216	6.8426	6.5317	6.2581	6.0202
		5.5650	5.1250	4.7401	4.4031	4.0928	3.8059	3.5254	3.2909	
53	I	9.6422	9.1056	8.6831	8.3551	7.9584	7.6306	7.3421	7.0258	6.7741
		6.2836	5.8591	5.4556	5.0838	4.7453	4.4476	4.1595	3.9002	
57	LA	11.6200	11.0909	10.6303	10.1350	9.7425	9.3073	8.9637	8.6106	8.2968
		7.7315	7.2254	6.7693	6.3422	5.9646	5.6144	5.2813	4.9833	
58	CE	11.4894	10.9460	10.5122	10.0288	9.6359	9.2402	8.8656	8.5562	8.2289
		7.6787	7.1910	6.7468	6.3326	5.9523	5.6157	5.2869	4.9811	
64	GD	11.9957	11.4600	11.0329	10.5967	10.2245	9.8649	9.4819	9.1841	8.8624
		8.3220	7.8415	7.3944	6.9822	6.6076	6.2605	5.9345	5.6351	
70	YB	12.0252	11.5305	11.1428	10.7483	10.3436	10.0665	9.7133	9.4184	9.1284
		8.5982	8.1509	7.7170	7.3189	6.9550	6.6196	6.3096	6.0174	
74	W	12.5569	12.1504	11.7813	11.3239	10.9935	10.6783	10.3303	10.0274	9.7497
		9.2114	8.7382	8.3088	7.9078	7.5280	7.1859	6.8713	6.5722	
76	OS	12.8359	12.4158	12.0424	11.6109	11.2547	10.9740	10.6219	10.3022	10.0360
		9.4885	9.0202	8.5885	8.1705	7.7954	7.4539	7.1305	6.8183	
78	PT	13.1248	12.7441	12.3083	11.8942	11.5823	11.2487	10.9034	10.6135	10.3072
		9.7937	9.3002	8.8599	8.4476	8.0702	7.7199	7.3916	7.0878	
80	HG	13.5611	13.0062	12.5998	12.2395	11.8503	11.5302	11.2065	10.9026	10.6126
		10.0773	9.5912	9.1331	8.7092	8.3387	7.9918	7.6568	7.3423	
82	PB	14.3165	13.7561	13.3507	12.9237	12.5148	12.1799	11.8216	11.5009	11.1963
		10.6319	10.1103	9.6426	9.2027	8.8174	8.4533	8.1012	7.7740	

(in k) while diminish somewhat in peak height. Finally, for elements with $72 \lesssim Z \lesssim 82$, a third peak starts to come in from the low k region. The three peaks and the two valleys move to higher k values as Z increases.

The positions of the peaks and valleys of the amplitude functions of some representative elements are plotted as a function of atomic number Z in Figure 8. It is readily apparent that roughly linear relationships exist for each peak and valley. Periodic deviations from such linear relationships are probably due to variation in electronic configurations. However, such deviations are not very significant in comparison to the present accuracy of EXAFS data. Nevertheless, the simple linear trends of these peaks and valleys in the backscattering amplitudes allow chemical identification of unknown elements and differentiation of different elements with sufficiently different Z values, as well as interpolation or extrapolation for elements not calculated in the present study. The equations describing the peaks (P_i) and valleys (V_i) for the first ($i = 1$) and the second ($i = 2$) amplitude envelopes are

$$P_1 = 0.204(Z + 8) \quad (7a)$$

$$V_1 = 0.136Z \quad (7b)$$

$$P_2 = 0.136(Z - 21) \quad (7c)$$

$$V_2 = 0.136(Z - 39) \quad (7d)$$

It is interesting to note that the slope of P_1 is 1.5 times the slopes of P_i and V_i where $i \neq 1$. Furthermore, with the exception of P_1, each peak and valley seem to start at the beginning of some series: V_1 with $Z = 0$, P_2 with $Z = 21$ (first transition series), and V_2 with $Z = 39$ (second transition series).

Scatterer Phase. Figures 4a–c depict the backscattering phase shifts for three groups while Figures 5a–d show the scatterer phase variation for series of elements in the periodic table. These plots exhibit a considerable amount of scatter, especially at low k and for the heavier elements like the rare earths. These scatters are systematic and are due to the truncation of the atomic wave function at the muffin tin radius r_{mt}. Such a truncation introduces a discontinuity in the exchange and correlation potential at the muffin tin radius which in turn introduces oscillations with period $2kr_{mt}$ in the phase shifts. It should be perfectly legitimate to smooth out such scatters in the tabulated phase shift before comparison is made with experiments. In practice, the scatter is small enough not to make too much difference.

At high enough k values, $\phi_b(k)$ decreases almost linearly with increasing k, whereas at low k values it exhibits complicated patterns which are related to the amplitude function $F(k)$. That is, above a certain energy, the phase shift decreases with increasing electron energy, whereas below such energy the phase shift depends heavily on the "resonance" interactions between the photoelectron and the various electronic shells of the scattering atom. A careful inspection of the low k region of $\phi_b(k)$ suggests that the plateau (slow varying regions) and the inflection points (fast varying regions) in the scatterer phase correspond to the peaks and valleys, respectively, in the scattering amplitude. These are illustrated in Figures 4a–c for three groups of elements where the P_i arrows designate the plateau and the V_i arrows represent the inflection points in $\phi_b(k)$. The P_i and V_i values (in k) are very similar to the corresponding values plotted in Figure 8.

It is interesting to note that the scatterer phase shift varies systematically with the atomic number Z. Within each shell, the phase shift increases linearly with Z as a result of the increasingly positive potential. In Figure 9 we plot the scatterer phase shift for $k = P_1$ (solid curve) and $k = 15.12$ Å^{-1} (dashed curve) as a function of atomic number Z. The former correspond to the phase shift at the photoelectron energy above which the phase shift decreases monotonically with increasing electron energy. It is immediately apparent that both curves vary linearly as a function of Z with breaks (changing slope) at $Z \simeq 21$ and 57 which correspond to the starts of the d and the f shells, respectively. Small but significant periodic deviations from the linear curves occur (especially for $k = 15.12$ Å^{-1} curve) due to the different electronic shells involved. Nevertheless, the $k = P_1$ curve can be used for chemical identification if the central atom phase shift (vide infra) can reliably be removed from the total phase shift.

The slope of the nearly linear or quadratic curve at $k \gtrsim P_1$ is also plotted as a function of Z in Figure 9. Here it varies linearly with Z only within each shell. The drastically different slopes for different shells produce discontinuities at the junctions. We have pointed out this phenomenon in our previous work on the parametrization of these phase functions (with $Z \lesssim 35$ only).[17b]

Central Atom Phase Shift. Central atom (or absorber) phase shift is a much simpler but perhaps stronger function of k. It generally decreases with increasing photoelectron energy (and hence k) as shown in Figures 6a–c for groups and Figures 7a–d for series of elements in the periodic table.

Again the central atom phase shift $\phi_a(k)$ varies systematically with increasing Z. In particular the potential is more

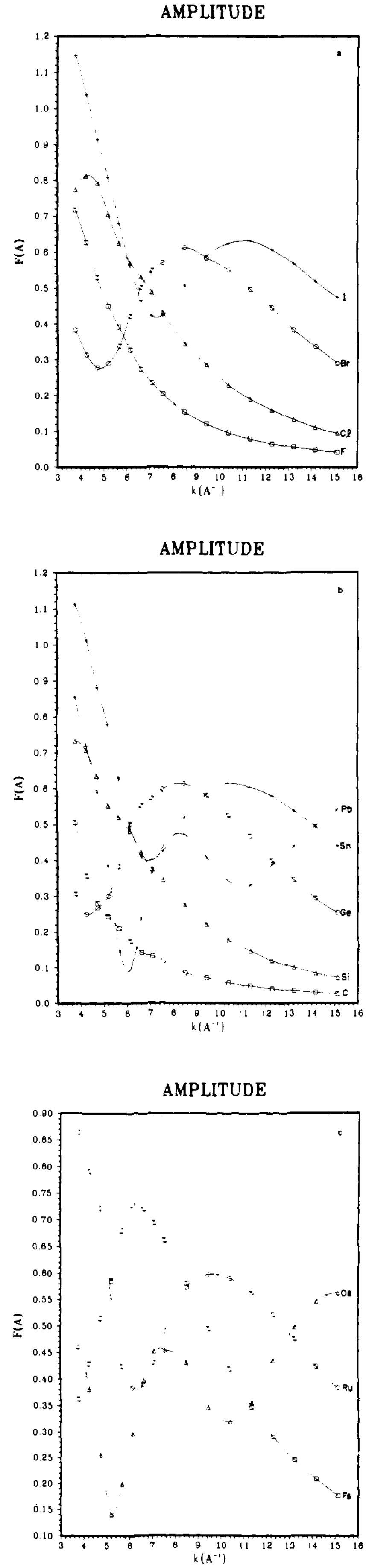

Figure 2. Backscattering amplitude functions for (a) group 7A elements; (b) group 4A elements; (c) transition metals Fe, Ru, and Os.

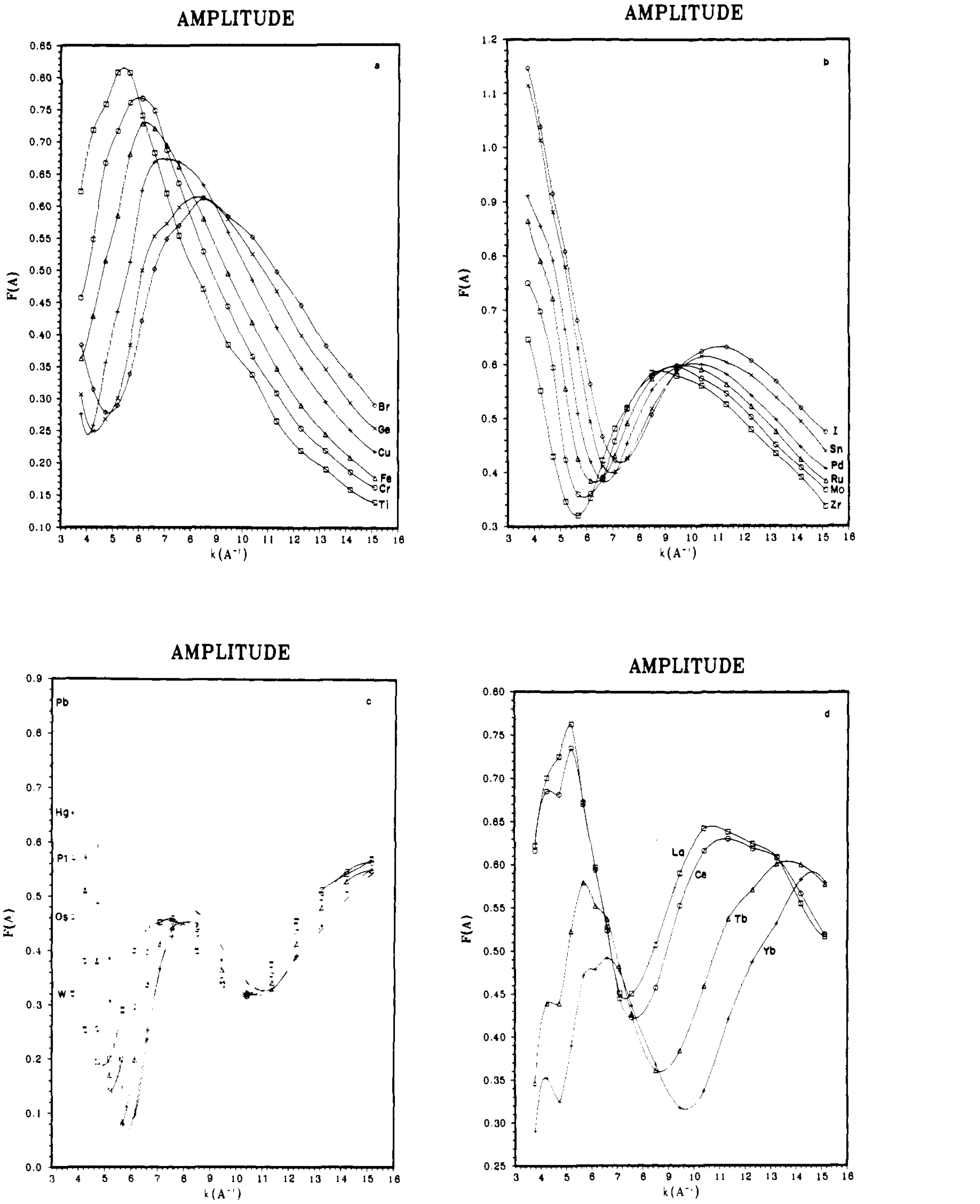

Figure 3. Backscattering amplitude functions for some representative elements in (a) first transition series and beyond; (b) second transition series and beyond; (c) third transition series and beyond; (d) lanthanides.

attractive for increasing Z and we expect that the phase shift should increase. This is indeed the case as exemplified in Figure 10, where we plot the central atom phase shifts for $k = 3.78$, 9.45, and 15.12 Å^{-1} as a function of Z. It is apparent that all three curves are reasonably linear in Z with, again, breaks at $Z \simeq 21$ and 57 which correspond to the injections of d and f electrons, respectively, into the electronic structure. The decreases in slope at these "break points" reflect the fact that the phase shift increases at slower rates for heavy elements than for light atoms. Once again, there are systematic deviations from these linear relations due to the different shells involved. Furthermore, the phase shifts at lower k regions increase much faster than the higher k regions as Z increases. At $Z \gtrsim 57$, however, all three curves approach similar slopes.

A comparison of the absorber phase shifts listed in Table III (calculated with Clementi-Roetti wave functions and the $Z + 1$ approximation) with those listed in Table VII (calculated with Herman-Skillman wave functions) for the same elements indicates that the former is more positive than the latter. This is apparently due to the more positive potential introduced by the $Z + 1$ approximation. Though the discrepancy between the two sets of phase shifts can in general be compensated by changing E_0, we recommend the use of Table VII whenever possible for consistency.

The E_0 Problem. It should be emphasized at this point that the phase shifts are unique only if the energy thresholds, E_0, are specified. Changing E_0 by $\Delta E_0 = E_0' - E_0$ will change the momentum k to

$$k' = \left(k^2 - \frac{2\Delta E_0}{7.62}\right)^{1/2} \tag{8}$$

where k is in Å^{-1} and ΔE_0 in eV. The corresponding modification of the phase shift function will be

$$\begin{aligned}\phi'(k') &= \phi(k) - 2(k' - k)r \\ &\simeq \phi(k) + 2r(\Delta E_0)/7.62k\end{aligned} \tag{9}$$

for $2(\Delta E_0)/7.62 \ll k^2$. As expected, the difference $\Delta\phi(k) = \phi'(k') - \phi(k)$ decreases with increasing k indicating that phase shifts are more sensitive to a change in E_0 at small k than at large k.

It is clear then that, in order to fit experimental data based upon some empirical E_0 with our theoretical phase shifts, we must allow E_0 to vary in such a way that $\Delta E_0 = E_0^{\text{th}} - E_0^{\text{exp}}$ with E_0^{th} and E_0^{exp} denoting the "theoretical" and "experimental" energy thresholds, respectively.

Since the determination of interatomic distance r depends on the precise knowledge of $\phi(k)$, the nonuniqueness of phase shifts naturally causes concern about the uniqueness of the distance determination. Fortunately, it can be shown that by adjusting E_0 it is not possible to produce an artificially good fit with a wrong distance r, simply because changing E_0 will affect $\phi(k)$ mainly at low k values by $\sim 2r(\Delta E_0)/(7.26k)$ whereas changing r will affect $\phi(k)$ mostly at high k values by $2k(\Delta r)$.[8]

Effect of Electronic Configuration. In this work we chose to use the atomic ground state electronic configuration for most elements. For example, the valence shell configurations for groups 4A and 7A are ns^2np^2 and ns^2np^5, respectively. For transition metals, we use the "majority" configurations of $3d^{Z-20}4s^2$, $4d^{Z-37}5s^1$, and $5d^{Z-70}6s^2$ for first, second, and third transition metal series, respectively, solely for the purpose of producing a smooth trend.

The small but significant effects of valence shell electronic configuration on the amplitude as well as the scatterer and central atom phase functions are illustrated in Figures 11a–c and 12a–c for Pd and Cu, respectively. The configurations used for Pd are $4d^85s^2$, $4d^95s^1$, and $4d^{10}5s^0$, whereas those used for Cu are $3d^94s^2$ and $3d^{10}4s^1$. It can be seen that the amplitude functions (Figures 11a and 12a) are little affected by changes in electronic configuration. The small variations at low k values are not unexpected because in this region the photoelectron energy is comparable to the valence shell binding energies. On the other hand, both the scatterer and the absorber phase shifts exhibit interesting systematic variations with electronic configuration. First, the scatterer phase (Figures 11b and 12b) increases with increasing population of the s orbital (or equivalently depopulation of the d orbitals). The difference between various configurations, however, diminishes as k increases. For example, it decreases from 0.35 rad at $k = 4$ Å^{-1} to 0.08 rad at $k = 15$ Å^{-1} for Pd. As pointed out in the foregoing section, this difference, which is roughly inversely proportional to k, can largely be compensated for by changing E_0.

The effect of valence shell electronic configuration on central atom phase function follows the same trend. Figure 11c depicts the $\phi_a{}^0(k)$, $\phi_a{}^1(k)$, and $\phi_a{}^2(k)$ functions for three different electronic configurations ($4d^{10-n}5s^n$ where $n = 0, 1, 2$) of Pd while Figure 12c shows the $\phi_a{}^1(k)$ functions for two different configurations ($3d^{10-n}4s^{n+1}$ where $n = 0, 1$) of Cu. In all cases, the phase shifts increase with increasing population of s orbital (or increasing depopulation of d orbitals). The difference, however, diminishes with increasing k (note that the

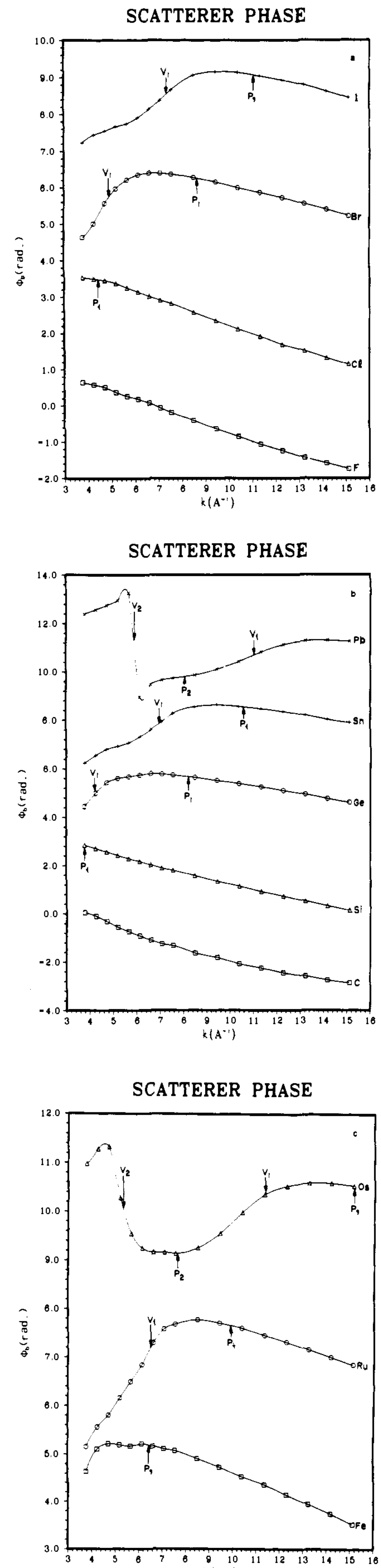

Figure 4. Backscattering phase functions for (a) group 7A elements; (b) group 4A elements; (c) transition metals Fe, Ru, and Os. The arrows P_i and V_i designate the "plateau" and the "inflection" points in $\phi_b(k)$ which correspond to the "peaks" and "valleys" in $F(k)$ (cf. Figure 2).

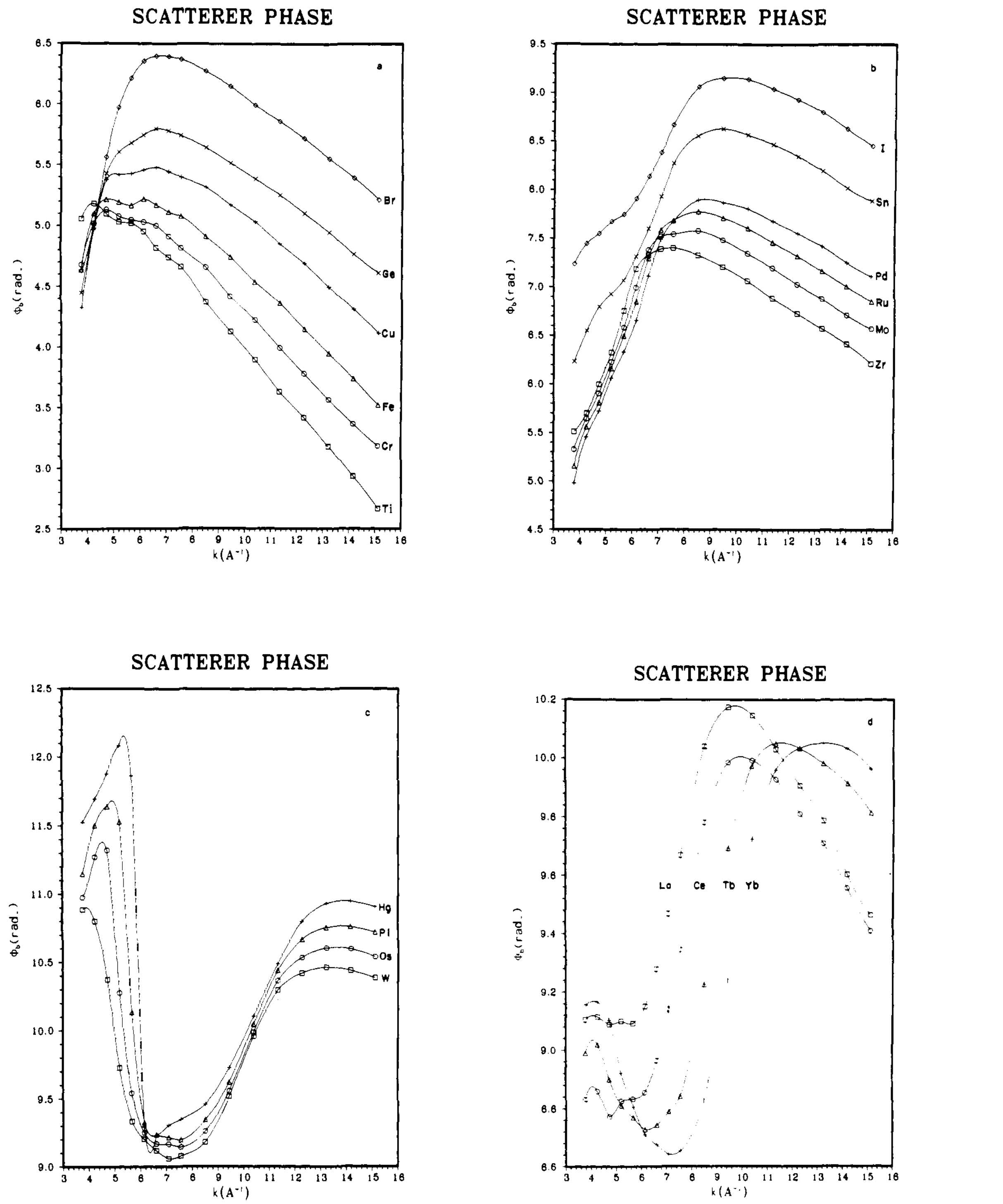

Figure 5. Backscattering phase functions for some representative elements in (a) first transition series and beyond; (b) second transition series and beyond; (c) third transition series and beyond; (d) lanthanides.

near parallel appearance of the phase functions is an optical illusion). For example, it decreases from ~0.25 and 0.55 rad at $k = 4$ Å^{-1} to 0.10 and 0.25 rad at $k = 15$ Å^{-1} for Pd and Cu, respectively. Again, such a difference can largely be compensated by E_0 variation as shown in Figure 12c for copper.

Charge Effect. Throughout this paper we use neutral atomic entities in our calculations except for a few alkali or alkali-earth metals which are treated as cations.

The effect of atomic charge on central atom phase shift has been explored for several elements. A typical example is shown in Figure 13. Here we plot $\phi_a{}^0$, $\phi_a{}^1$, and $\phi_a{}^2$ as a function of k for Ca and Ca^{2+}. It is immediately obvious that the dication not only has a more positive phase shift but also a larger slope. It is also readily apparent that the effect of atomic charge on phase shifts is significantly larger than that of electronic configuration. For example, at $k = 4$, 15 Å^{-1}, $\phi_a{}^1$ of Ca and Ca^{2+} are 0.20, −5.68 and 2.64, −4.85, respectively. This is not unexpected since the atomic charge exerts a significant effect on the central atom potential which is experienced by both the outgoing and the incoming photoelectrons. The difference, again, can partially be compensated by E_0 variation.

Comparison of $\phi_a{}^l$ (l = 0, 1, 2) Functions. The $\phi_a{}^l$ functions listed in Tables VI, VII, and VIII, where l = 0, 1, 2, are central atom (absorber) phase shifts for the excitations p → s ($L_{II,III}$

edges), s → p (K or L_I edge), and p → d ($L_{II,III}$ edges), respectively. Two examples are shown in Figure 11c for palladium and in Figure 13 for calcium. In both cases, there are large differences between the $\phi_a{}^l$ phase functions. The order $\phi_a{}^2 > \phi_a{}^1 > \phi_a{}^0$ as well as the divergence at large k values may not be physically meaningful since subtracting 2π from $\phi_a{}^2$ and adding 2π to $\phi_a{}^0$ yield an inverted order $\phi_a{}^2 < \phi_a{}^1 < \phi_a{}^0$ which converges at high k.

We have also investigated the difference in absorber phase shifts for exciting 1s (K edge) vs. 2s (L_I edge) and found no significant discrepancy between the two.

Relativistic Effect. We have obtained the charge density for tungsten calculated using relativistic wave functions from John H. Wood (Los Alamos). These were used as input to calculate the backscattering amplitude and phase. These are compared with the result using Herman-Skillman wave functions in Figure 14. We see that the amplitudes are in substantial agreement, especially beyond $k = 6$ Å^{-1}. The phase shows a systematic deviation which is progressively smaller for higher k. This kind of deviation is of the same order as that due to configuration differences and can be compensated for by changing E_0. Strictly speaking, for the heavier elements one should treat the electron scattering problem relativistically.[27] However, the relativistic corrections such as spin-orbit terms are small compared with the Hartree and exchange potential and we assume can again be compensated for by E_0 change.

EXAFS Data Analysis. In EXAFS analysis, it is often necessary to multiply the $\chi(k)$ data by a weighting scheme such as k^n in order to compensate for amplitude reduction as a function of k. For data in the range of $k = 4$–15 Å^{-1}, we recommend using the weighting schemes of $k^3\chi(k)$, $k^2\chi(k)$, and $k\chi(k)$ for backscatterers with atomic number $Z \lesssim 36$, $36 \lesssim Z \lesssim 57$, and $57 \lesssim Z \lesssim 86$, respectively. These weighting schemes appropriately emphasize the relative importance of different regions within the data without severely distorting the amplitude envelope. That is, for light scatterers with a rapidly attenuating backscattering amplitude (due partly to $F(k)$ and partly to the Debye-Waller factor) we suggest a larger n value in $k^n\chi(k)$ to bring out the high k region, whereas for heavy scatterers with strong backscattering power a small n value will help preserve the "fine structure" of the backscattering amplitude as well as the backscattering phase. Another reason for choosing an appropriate weighting scheme is that the scattering amplitude exhibits increasing number of peaks (in k space) with increasing atomic number Z which inevitably show up in the Fourier transforms of the EXAFS spectra and could be mistaken as a separate distance or the satellite peak from a neighboring edge. In fact, the resulting Fourier transform and the filtered EXAFS spectra are to some extent affected by the weighting scheme and Fourier-filtering window. Experience showed that, with too narrow a filtering window and an inappropriate weighting, some of the "fine structures" of the amplitude envelope could be "washed" away.

Our theoretical functions and their parametrized versions[17] have been used in EXAFS analysis of a wide variety of physical, chemical, and biological systems. The results are generally favorable. However, an overall scale factor of ca. 50% is often required in comparing the theoretical amplitude with experiment.[28] For single-shell systems, the accuracy for the distance r is better than 0.5% (~0.01 Å), for the Debye-Waller factor σ is better than 10%, and for the coordination number N is ~20%.[15-20] Somewhat worse accuracy is expected for multiatom multidistance systems, though for systems with significantly different Z scatterers interatomic distances can easily be determined to within 0.03 Å.[16-20]

Our previous work has been restricted to atoms with $Z < 36$. In order to illustrate the situation for heavier elements, we compare the calculated Pt-Pt phase shift and amplitude with

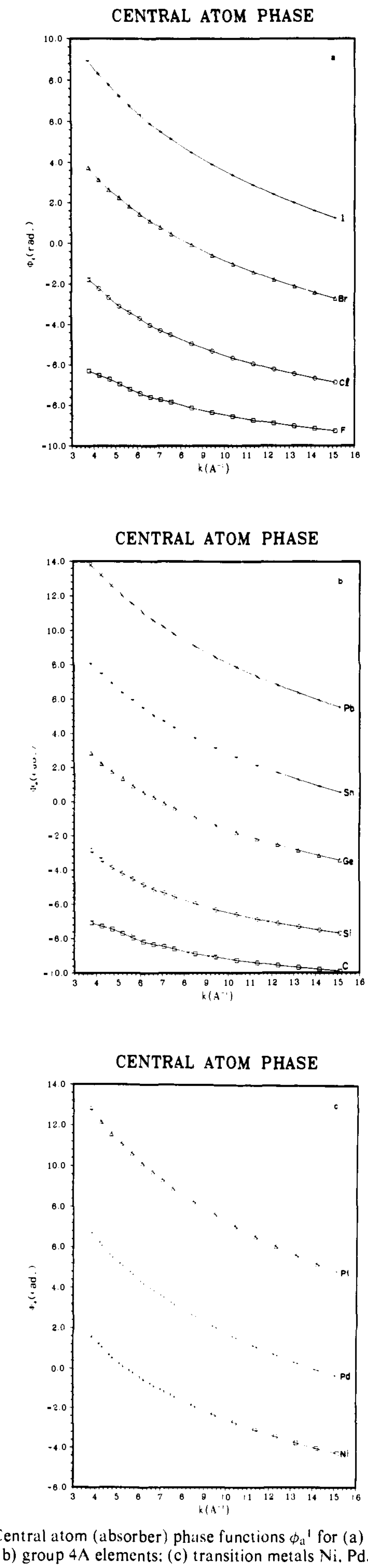

Figure 6. Central atom (absorber) phase functions $\phi_a{}^1$ for (a) group 7A elements; (b) group 4A elements; (c) transition metals Ni, Pd, and Pt.

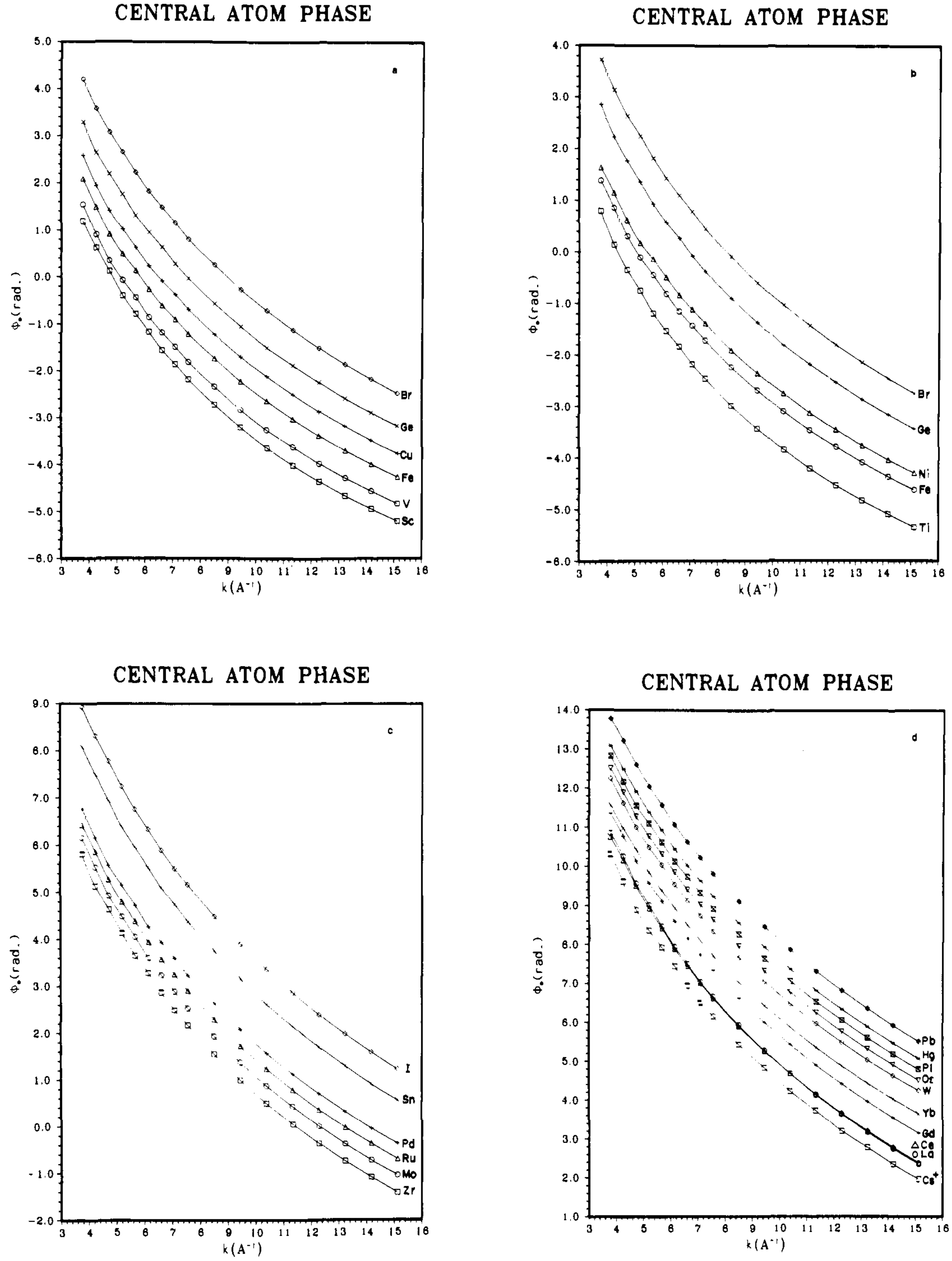

Figure 7. Central atom (absorber) phase functions $\phi_a{}^1$ for some representative elements in (a) first transition series and beyond (Clementi-Roetti wave functions); (b) first transition series and beyond (Herman-Skillman wave functions); (c) second transition series and beyond; (d) third transition series, lanthanides, etc.

the first shell of platinum metal. Figure 15a shows the $k\chi(k)$ data of platinum metal ($L_{\rm I}$ edge) after the "approximate" normalization with edge jump and Victoreen's true absorption coefficient $\mu_0/P = C\lambda^3 - D\lambda^4$ (where $C = 470$, $D = 219$)[29] and a cubic spline background removal with four sections. The energy threshold E_0 was arbitrarily chosen as 13 900 eV, which corresponds to the first sharp peak at the edge. The Fourier transform is shown in Figure 15b. A smooth filtering window of 1.6-3.8 Å which encompasses the two major peaks (2.0 and 2.5 Å) was used to remove the higher shells as well as the high-frequency noise and the low-frequency residual peaks. The Fourier peaks at 1.2 and 1.65 Å (the former disappears when the data set is truncated at k = 3-14 Å^{-1}) may be due to residual EXAFS from the $L_{\rm II}$ edge which is 608.9 eV lower in energy. The resulting Fourier filtered spectrum is shown as a dashed curve in Figure 15a. Figure 15c shows the comparison between the experimental amplitude and our theoretical function $NF(k)e^{-2\sigma^2k^2}$ with an overall scale[28] factor $N = 0.54$ and a Debye-Waller factor $\sigma = 0.05$ Å (note that $e^{-2r/\lambda}$ was set to unity). The double peaks (ca. 0.5 Å apart) observed for each shell are a consequence of the characteristic structure of the amplitude functions of heavy scatterers. The agreement

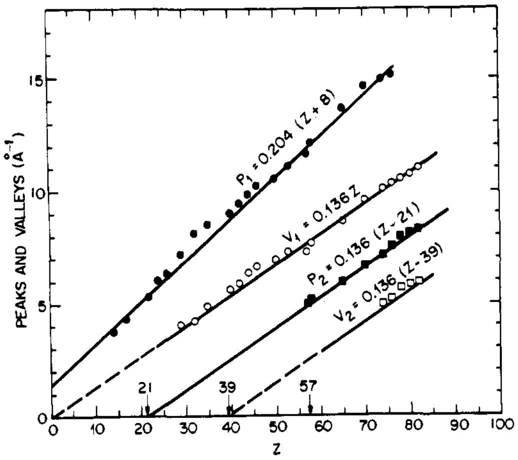

Figure 8. The positions (in k space) of the peaks (P_i) and valleys (V_i) of the amplitude functions vs. atomic number Z.

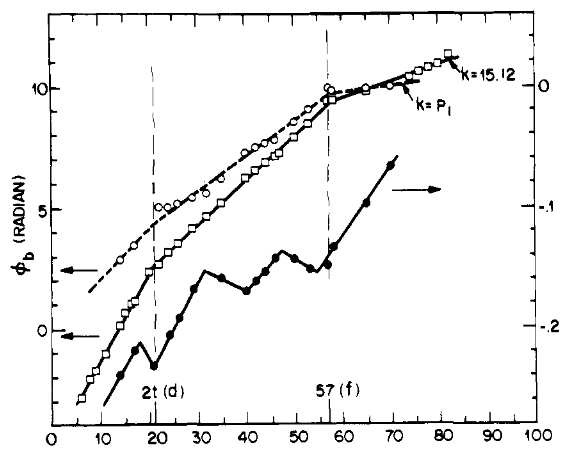

Figure 9. Backscattering phase shift ϕ_b (rad) at $k = P_1$ (open circles) and $k = 15.12$ Å^{-1} (open squares) vs. atomic number Z. The slope of ϕ_b for $k \lesssim P_1$ is also plotted (filled circles) as a function of Z.

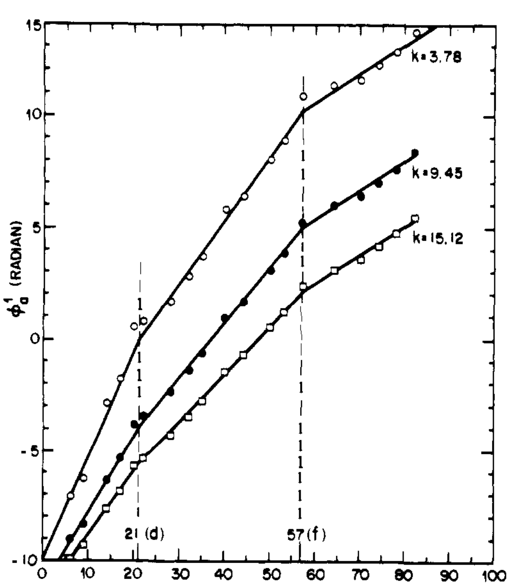

Figure 10. Central atom (absorber) phase shift $\phi_a{}^1$ (radian) at $k = 3.78$ (open circles), 9.45 (filled circles), and 15.12 (open squares) Å^{-1} vs. atomic number Z.

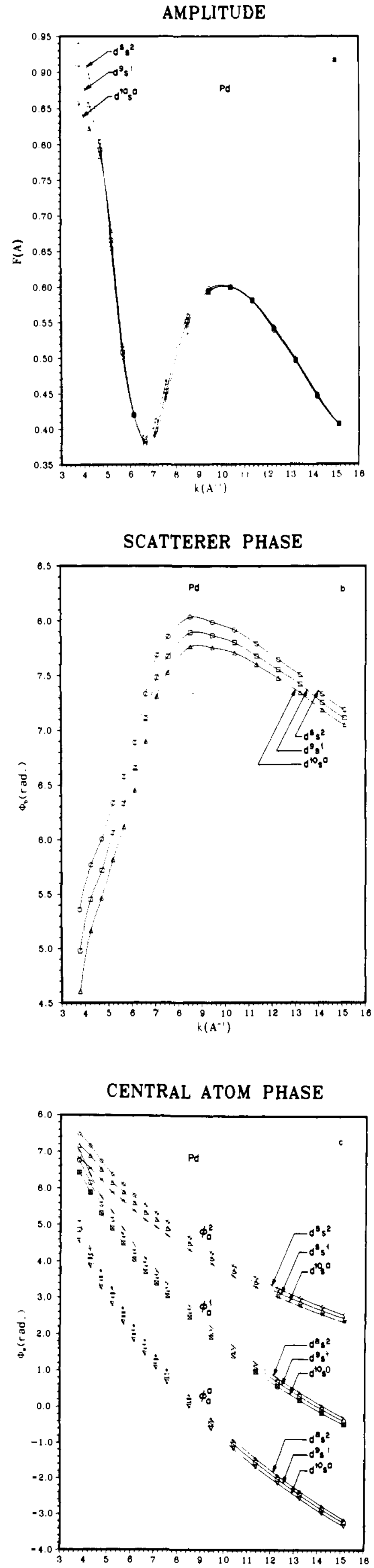

Figure 11. Comparisons of the amplitude (a), backscattering phase (b), and central atom phase (c) functions for Pd with electronic configurations $4d^85s^2$, $4d^95s^1$, and $4d^{10}5s^0$.

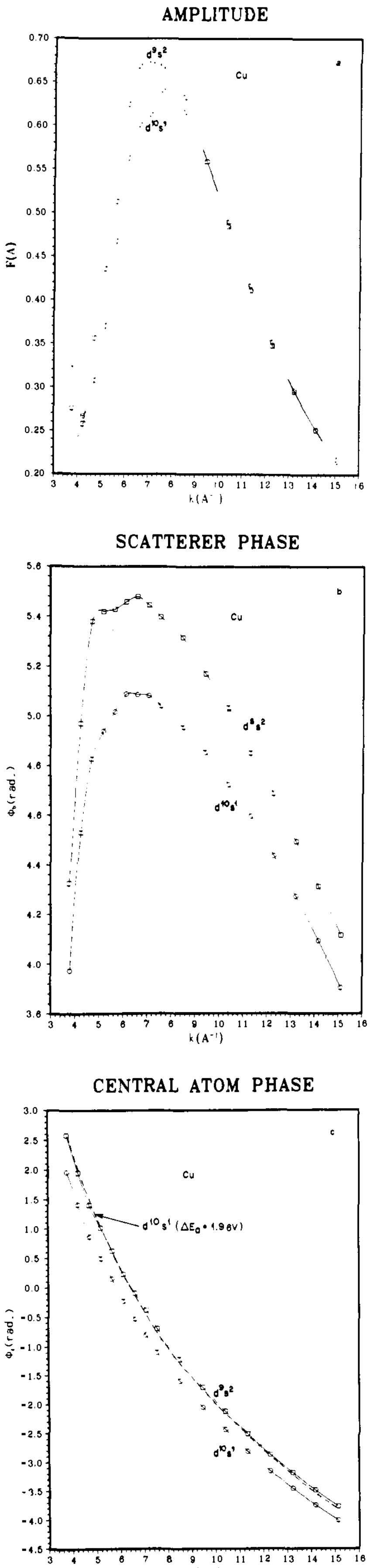

Figure 12. Contrasts of the amplitude (a), backscattering phase (b), and central atom phase $\phi_a{}^1$ (c) functions for Cu with electronic configurations $3d^94s^2$ and $3d^{10}4s^1$. In (c), the dashed line corresponds to $d^{10}s^1$ phase with $\Delta E_0 = 1.9$ eV.

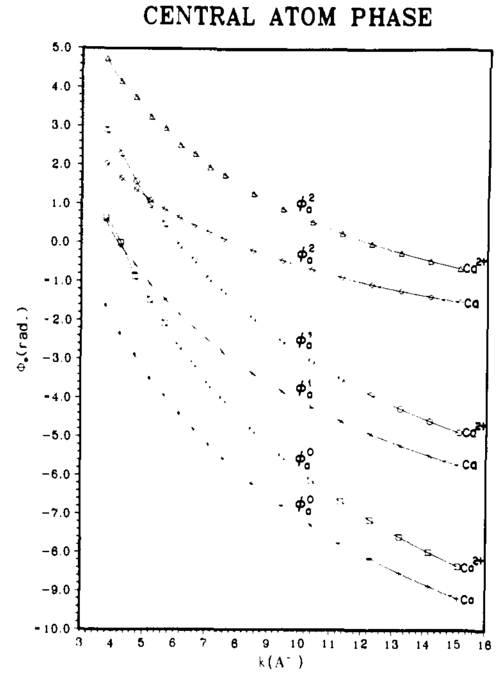

Figure 13. The effect of atomic charge on the central atom phase shifts as exemplified by Ca and Ca^{2+}.

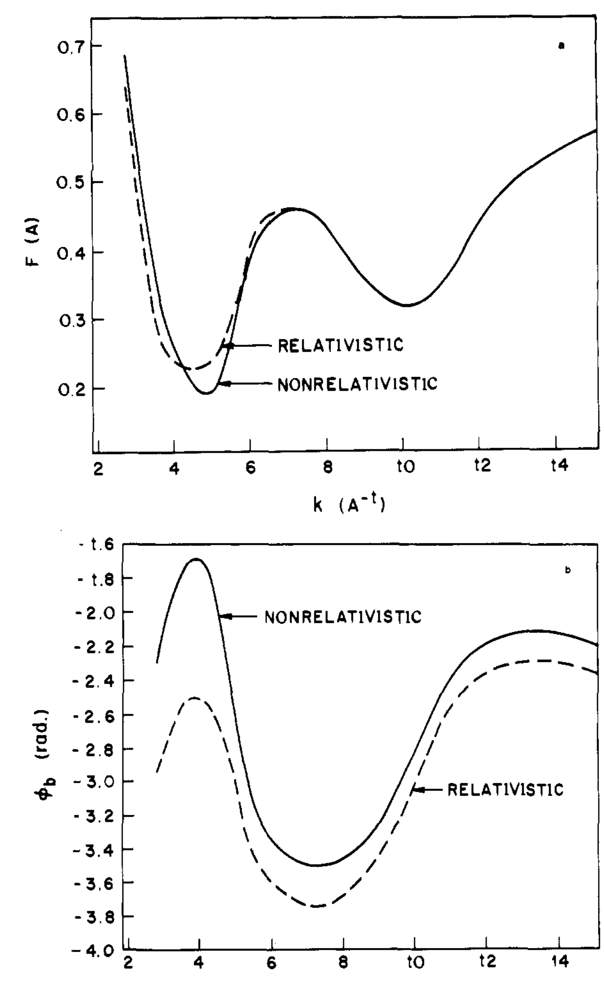

Figure 14. Relativistic effects on the amplitude (a) and scatterer phase (b) functions as exemplified by a calculation on W using relativistic (dashed curves) vs. nonrelativistic (solid curves) wave functions.

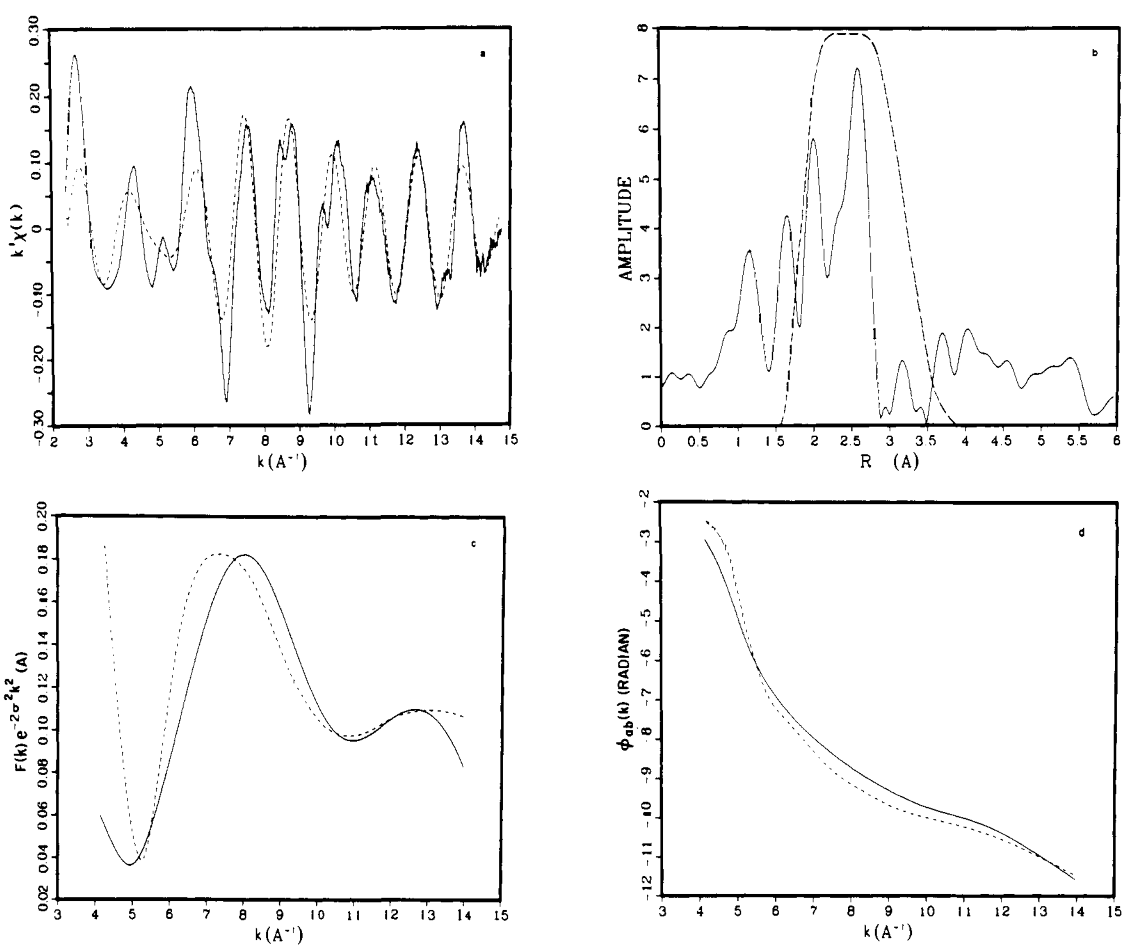

Figure 15. (a) Unfiltered (solid curve) and Fourier filtered (dashed curve) $k\chi(k)$ vs. k EXAFS data (L_I edge) of Pt metal after an "approximate" normalization with the edge jump and Victoreen's true absorption coefficient (see text) and a cubic spline background removal with four sections; (b) Fourier transform (solid curve) and the filtering window (dashed curve) of the unfiltered $k\chi(k)$ vs. k data; (c) experimental Pt backscattering amplitude function (solid curve) is fitted with the theoretical function (dashed curve) $NF(k)e^{-2\sigma^2k^2}$ where $N = 0.54$ and $\sigma = 0.05$ Å; (d) experimental Pt-Pt phase shift (solid curve) is compared with the theoretical phase function (dashed curve) $\phi_{ab} = \phi_a + \phi_b - 9\pi$ where both a and b refer to Pt. In both (c) and (d), the theoretical energy threshold has been moved by 16 eV (viz., $E_0^{exp} - E_0^{th} = 16$ eV).

is fairly good with the exception of low k regions. While theoretical amplitudes are generally found to be too high at low k values, it should be noted that the Fourier filtering with a reasonable window often causes a reduction of amplitude at low and high k regions (cf. Figure 15a). Figure 15d illustrates the good agreement between the experimental Pt-Pt phase shift (after subtracting the $2kR$ contribution where $R = 2.775$ Å)[30] and the theoretical function calculated by $\phi_{ab} = \phi_a + \phi_b - 9\pi$ (where both a and b refer to platinum). It should be noted that the somewhat complicated structure (deviation from the almost quadratic k dependence) of the phase function arises from the heavy scatterer platinum (cf. Figure 5c). It should also be mentioned that in Figures 15c and d, the theoretical energy threshold has been moved by 16 eV ($\Delta E_0 = E_0^{exp} - E_0^{th}$). Good agreements have also been observed with K and L edges of other elements.[31]

In conclusion, our theoretical amplitude and phase functions are adequate for EXAFS data analysis for heavy elements with atomic number $Z \lesssim 82$. These functions, or the parametrized versions, can be used not only to determine interatomic distances, Debye-Waller factors, and coordination numbers, but also to identify unknown chemical types in complicated systems, without resorting to searching, measuring, and analyzing model compounds. When coupled with the existing techniques such as Fourier transform and curve fitting, they greatly enhance the chemical content of EXAFS spectroscopy.

Acknowledgments. We thank A. L. Simons and B. Chambers for assistance in the programming.

References and Notes

(1) R. de L. Kronig, *Z. Phys.*, **70**, 317 (1931); **75**, 191, 468 (1932).
(2) E. A. Stern, *Phys. Rev. B*, **10**, 3027 (1974).
(3) D. E. Sayers, F. W. Lytle, and E. A. Stern, *Adv. X-Ray Anal.* **13**, 248 (1970).
(4) (a) D. E. Sayers, E. A. Stern, and F. W. Lytle, *Phys. Rev. Lett.*, **27**, 1204 (1971); (b) F. W. Lytle, D. E. Sayers, and E. A. Stern, *Phys. Rev. B*, **11**, 4825 (1975); (c) E. A. Stern, D. E. Sayers, and F. W. Lytle, *ibid.*, **11**, 4836 (1975), and references cited therein.
(5) (a) D. E. Sayers, E. A. Stern, and F. W. Lytle, *Phys. Rev. Lett.*, **35**, 584 (1975); (b) D. E. Sayers, F. W. Lytle, M. Weissbluth, and P. Pianetta, *J. Chem. Phys.*, **62**, 2514 (1975); (c) F. W. Lytle, D. E. Sayers, and E. B. Moore, Jr., *Appl. Phys. Lett.*, **24**, 45 (1974).
(6) C. A. Ashley and S. Doniach, *Phys. Rev. B*, **11**, 1279 (1975).
(7) P. A. Lee and J. B. Pendry, *Phys. Rev. B*, **11**, 2795 (1975).
(8) P. A. Lee and G. Beni, *Phys. Rev. B*, **15**, 2862 (1977).
(9) B. M. Kincaid and P. Eisenberger, *Phys. Rev. Lett.*, **34**, 1361 (1975).
(10) P. H. Citrin, P. Eisenberger, and B. M. Kincaid, *Phys. Rev. Lett.*, **36**, 1346 (1976).
(11) (a) B. M. Kincaid, P. Eisenberger, K. O. Hodgson, and S. Doniach, *Proc. Natl. Acad. Sci. U.S.A.*, **72**, 2340 (1975); (b) P. Eisenberger and B. M. Kincaid, *Chem. Phys. Lett.*, **36**, 134 (1975).
(12) P. Eisenberger and B. M. Kincaid, *Science*, **200**, 1441 (1978).
(13) R. E. Watson and M. L. Perlman, *Science*, **199**, 1295 (1978).
(14) (a) R. G. Shulman, P. Eisenberger, W. E. Blumberg, and N. A. Stombaugh, *Proc. Natl. Acad. Sci. U.S.A.*, **72**, 4003 (1975); (b) P. Eisenberger, R. G. Shulman, G. S. Brown, and S. Ogawa, *ibid.*, **73**, 491 (1976).
(15) R. G. Shulman, P. Eisenberger, B. K. Teo, B. M. Kincaid, and G. S. Brown, *J. Mol. Biol.*, **124**, 305 (1978).
(16) B. K. Teo, R. G. Shulman, G. S. Brown, and A. E. Meixner, submitted for publication.

(17) (a) B. K. Teo, P. A. Lee, A. L. Simons, P. Eisenberger, and B. M. Kincaid, *J. Am. Chem. Soc.*, **99**, 3854 (1977); (b) P. A. Lee, B. K. Teo, and A. L. Simons, *ibid.*, **99**, 3856 (1977).
(18) B. K. Teo, P. Eisenberger, and B. M. Kincaid, *J. Am. Chem. Soc.*, **100**, 1735 (1978).
(19) (a) B. K. Teo, K. Kijima, and R. Bau, *J. Am. Chem. Soc.*, **100**, 621 (1978); (b) B. K. Teo, P. Eisenberger, J. Reed, J. K. Barton, and S. J. Lippard, *ibid.*, **100**, 3225 (1978).
(20) (a) J. Reed, P. Eisenberger, B. K. Teo, and B. M. Kincaid, *J. Am. Chem. Soc.*, **99**, 5217 (1977); (b) J. Reed, P. Eisenberger, B. K. Teo, and B. M. Kincaid, *ibid.*, **100**, 2375 (1978).
(21) (a) S. P. Cramer, T. K. Eccles, F. Kutzler, K. O. Hodgson, and S. Doniach, *J. Am. Chem. Soc.*, **98**, 8059 (1976); (b) S. P. Cramer and K. O. Hodgson, *ibid.*, **100**, 2748 (1978).
(22) For example, if one arbitrarily defines ϕ_a of atom A (absorber), one can deduce ϕ_b of atom B (scatterer) from the experimental phase shift ϕ_{ab} for the atomic pair A–B. From ϕ_b one can then determine the central atom phase $\phi_{a'}$ of any atom A′ by measuring $\phi_{a'b}$ which is the total phase shift of atom pair A′B where A′ and B denote the (new) absorber and the (old) scatterer, respectively. Similarly, from ϕ_a it is possible to deduce the scatterer phase $\phi_{b'}$ of any atom B′ by measuring $\phi_{ab'}$ for the atom pair AB′ with A and B′ being the (old) absorber and the (new) scatterer, respectively. All individual phase functions constructed in this manner are "relative" to the arbitrarily defined ϕ_a of absorber A.
(23) S. M. Heald and E. A. Stern, *Phys. Rev. B*, **16**, 5549 (1977).
(24) In the matrix element the initial state should be that of a neutral atom and the final state that of an ion with a 2p hole. In our calculation, it is more convenient to use either the neutral atom or the ion wave functions for both the initial and final states. The ratios M_{21}/M_{01} obtained using these two methods are found to be in agreement to within a few percent even though the individual matrix elements show bigger variation. The result using the ion wave functions has been plotted in Figure 1. We should also mention that there is a considerable amount of literature dealing with M_{21}/M_{01} for light elements or outer shells. See, for instance, O. J. Kennedy and S. T. Manson, *Phys. Rev. A*, **5**, 227 (1972); K. Codling, R. G. Houlgate, J. B. West, and P. R. Woodruff, *J. Phys. B*, **9**, L83 (1976).
(25) F. W. Lytle, D. E. Sayers, and E. A. Stern, *Phys. Rev. B*, **15**, 2426 (1977).
(26) (a) E. Clementi and C. Roetti, *At. Data Nucl. Data Tables*, **14**, 177 (1974); (b) F. Herman and S. Skillman, "Atomic Structure Calculations", Prentice-Hall, Englewood Cliffs, N.J., 1963.
(27) N. F. Mott, *Proc. R. Soc. London, Ser. A*, **124**, 425 (1925); **135**, 429 (1932); M. Fink and A. C. Yates, *At. Data*, **1**, 385 (1970).
(28) The theoretical amplitude functions, which include inelastic processes in the scattering atom, are found to be off by ~50%. Part of this discrepancy is due to core relaxation effects. Furthermore, the amplitude is expected to be somewhat sensitive to the chemical environment and will depend on the distance r_i (due to an exponential damping factor $e^{-2r_i/\lambda}$). An overall scale factor is therefore included in the refinements.
(29) "International Tables for X-ray Crystallography", Vol. III, Kynoch Press, Birmingham, England, 1968, pp 161, 172.
(30) L. Pauling, "The Nature of the Chemical Bond", 3rd ed., Cornell University Press, Ithaca, N.Y., 1960, p 403.
(31) P. Rabe, G. Tolkiehn, and A. Werner, *J. Phys. C*, in press.

Resonance Raman Spectroelectrochemistry. 6. Ultraviolet Laser Excitation of the Tetracyanoquinodimethane Dianion

Richard P. Van Duyne,*[1a,b] Mary R. Suchanski,[1c] Joseph M. Lakovits,[1a] Allen R. Siedle,[1d] Keith D. Parks,[1a] and Therese M. Cotton[1a,e]

Contribution from the Department of Chemistry, Northwestern University, Evanston, Illinois 60201, and the Central Research Laboratories, 3M Company, St. Paul, Minnesota 55101. *Received November 27, 1978*

Abstract: The resonance Raman spectrum has been obtained for the electrogenerated dianion of tetracyanoquinodimethane (TCNQ) upon excitation of its lowest energy electronic transition (λ_{max} 330 nm) with a frequency doubled, flashlamp-pumped, Rhodamine 640 dye laser. For comparison we report the normal Raman spectrum of solid $Li_2TCNQ{\cdot}THF$. The electron transfer induced frequency shifts for the second reduction step of TCNQ are measured and interpreted using the π-bond order changes determined from SCF-MO-CI and INDO/S electronic structure calculations as well as the π-bond length changes determined from a MNDO-SCF-MO calculation. Finally, the $TCNQ^{2-}$ Raman data is used to identify the oxidation state of TCNQ in the coordination complex $[Co(acacen)(py)_2]_2TCNQ$.

Introduction

It is now widely recognized that the observables in resonance Raman spectroscopy (RRS) (viz., vibrational frequency, resonance-enhanced vibrational symmetry type, number and intensity pattern of overtones, and depolarization ratios) and their laser excitation wavelength dependence represent sensitive probes of the molecular and electronic structure changes that can occur in molecules. Such structure changes are commonly induced by chemical modification, electron-transfer (ET) reactions, and optical excitation. Our primary motivation for applying RRS to the study of molecular and electronic structure changes stems from a long-term interest in developing a detailed description of ET processes. In particular we have been concerned with evaluating the role of intramolecular vibrational energy dissipation processes in highly exothermic, homogeneous, ET reactions.[2-7] To compare such ET theories with experiment, information is needed concerning the magnitude of the specific structural changes (viz., bond length, vibrational frequency, and anharmonicity) which occur within the donor and acceptor molecules during an ET process. In addition we are interested in studying the molecular and/or electronic structure changes that accompany the partial ET reactions involved in the formation of donor-acceptor, charge-transfer complexes that behave as one-dimensional, organic, electrical conductors.[8-12,41] Thus the technique of resonance Raman spectroelectrochemistry (RRSE) was developed[13] as a convenient means of coupling the observational sensitivity of RRS for monitoring molecular and electronic structure changes with the ability of electrochemistry to initiate and cleanly carry out successive one-electron transfer reactions.

Tetracyanoquinodimethane (TCNQ) was chosen for study by RRSE because it is a strong electron-acceptor molecule,[8] is the acceptor half of the prototype one-dimensional, organic metal tetrathiafulvalene-tetracyanoquinodimethane[8,9] (TTF-TCNQ) and exhibits two successive, one-electron reductions that are both chemically and electrochemically reversible in deoxygenated, aprotic solvents:[14]

$$TCNQ^0\,(^1A_g) + e^- \rightleftharpoons TCNQ^{-}\cdot(^2B_{3g}) \qquad (1)$$

$$TCNQ^{-}\cdot(^2B_{3g}) + e^- \rightleftharpoons TCNQ^{2-}(^1A_g) \qquad (2)$$

RRSE with visible ion laser lines has been used to obtain the RRS of the $^2B_{3g}$ (viz., D_{2h} point group) ground state of the

0002-7863/79/1501-2832$01.00/0